AGU PUBLICATIONS

Water Resources Research

RESEARCH ARTICLE
10.1002/2015WR016902

Key Points:
- The multirate mass transfer model combines subordination to streamlines
- Fractional advection-dispersion equation to capture retention and early arrivals
- Lagrangian solvers for multirate mass transfer with different memory functions

Correspondence to:
Y. Zhang,
yzhang264@ua.edu

Citation:
Zhang, Y., M. M. Meerschaert, B. Baeumer, and E. M. LaBolle (2015), Modeling mixed retention and early arrivals in multidimensional heterogeneous media using an explicit Lagrangian scheme, *Water Resour. Res.*, *51*, 6311–6337, doi:10.1002/2015WR016902.

Received 10 JAN 2015
Accepted 14 JUL 2015
Accepted article online 21 JUL 2015
Published online 14 AUG 2015

Modeling mixed retention and early arrivals in multidimensional heterogeneous media using an explicit Lagrangian scheme

Yong Zhang[1], Mark M. Meerschaert[2], Boris Baeumer[3], and Eric M. LaBolle[4]

[1]Department of Geological Sciences, University of Alabama, Tuscaloosa, Alabama, USA, [2]Department of Statistics and Probability, Michigan State University, East Lansing, Michigan, USA, [3]Department of Mathematics and Statistics, University of Otago, Dunedin, New Zealand, [4]Department of Land, Air, and Water Resources, University of California, Davis, California, USA

Abstract This study develops an explicit two-step Lagrangian scheme based on the renewal-reward process to capture transient anomalous diffusion with mixed retention and early arrivals in multidimensional media. The resulting 3-D anomalous transport simulator provides a flexible platform for modeling transport. The first step explicitly models retention due to mass exchange between one mobile zone and any number of parallel immobile zones. The mobile component of the renewal process can be calculated as either an exponential random variable or a preassigned time step, and the subsequent random immobile time follows a Hyper-exponential distribution for finite immobile zones or a tempered stable distribution for infinite immobile zones with an exponentially tempered power-law memory function. The second step describes well-documented early arrivals which can follow streamlines due to mechanical dispersion using the method of subordination to regional flow. Applicability and implementation of the Lagrangian solver are further checked against transport observed in various media. Results show that, although the time-nonlocal model parameters are predictable for transport with retention in alluvial settings, the standard time-nonlocal model cannot capture early arrivals. Retention and early arrivals observed in porous and fractured media can be efficiently modeled by our Lagrangian solver, allowing anomalous transport to be incorporated into 2-D/3-D models with irregular flow fields. Extensions of the particle-tracking approach are also discussed for transport with parameters conditioned on local aquifer properties, as required by transient flow and nonstationary media.

1. Introduction

Anomalous transport with retention or early arrivals have been well documented in many disciplines, motivating the development of nonlocal physical models such as the fractional advection-dispersion equation (fADE) [*Metzler and Klafter*, 2000, 2004; *Kilbas et al*., 2006; *Herrmann*, 2011]. In hydrology, anomalous diffusion due to retention has been observed for tracers transport in soils [*Pachepsky et al*., 2000; *Levy and Berkowitz*, 2003; *Bromly and Hinz*, 2004; *Cortis and Berkowitz*, 2004; *Delay et al*., 2005; *Hunt et al*., 2013], rocks [*LaBolle and Fogg*, 2001; *Kosakowski*, 2004; *Pedretti et al*., 2013; *Ronayne*, 2013], and streams [*Czernuszenko et al*., 1998; *González-Pinzón et al*., 2013], while anomalous diffusion with early arrivals has been found for conservative tracer transport in soils [*Zhang et al*., 2014a], streams [*Deng et al*., 2004, 2006; *Kim and Kavvas*, 2006], bed load or suspended sediment transport in rivers [*Stark et al*., 2009; *Houssais and Lajeunesse*, 2012, among many others], and solutes moving along fractured media at various scales [*Benson et al*., 2001; *Reeves et al*., 2008a, 2008b; *Zhang et al*., 2013]. The fADE is found to be superior to the second-order advection-dispersion equation (ADE) in quantifying the observed non-Fickian transport behavior [*Benson et al*., 2000, 2004; *Schumer et al*., 2009; *Zhang et al*., 2009]. In particular, the time fADE captures a heavy-tailed retention process, where the mass exchange between the mobile zone and parallel immobile zones has an infinite number of rates which distribute as a power-law function [*Schumer et al*., 2003a; *Zhang et al*., 2008]. In addition, the multidimensional space fADE describes early arrivals that exceed the early time mass growth rate predicted by Fickian diffusion models [*Meerschaert et al*., 2001; *Schumer et al*., 2003b; *Zhang et al*., 2008]. After *Benson et al*. [2000] first introduced the concept of fADE to the hydrology community, the fractional engine has been increasingly used by hydrologists as a promising modeling tool for various

hydrologic processes. For example, fractional-derivative models were recently used to explore anomalous diffusion observed in fine particulate organic carbon transport in rivers [*Drummond et al*., 2014], rainfall properties [*Golder et al*., 2014], groundwater travel time distributions [*Green et al*., 2014], flow or transport in heterogeneous porous or fractured media [*Heidari and Li*, 2014], water wave propagation and flow in pipes [*Jennings et al*., 2014; *Tarasov*, 2014], and sediment transport in rivers [*Sun et al*., 2015, among many others].

A revision of the above standard fractional engine, however, is needed to address numerical challenges related to complex transport dynamics in natural geological media. First, the capability of immobile blocks in retarding solute movement depends on physical and chemical properties of the host medium, where the number of the Mobile/IMmobile (MIM) mass exchange rate coefficients can vary from one to infinite and the distribution of rate coefficients is not limited to be power-law [*Haggerty et al*., 2000]. Laboratory experiments also revealed that the desorption rates of radionuclides from volcanic rocks are very widely distributed, yielding a $3 \sim 4$ order of magnitude range of desorption rate constants [*Dean and Reimus*, 2008]. Second, early arrivals can be observed for tracer transport through highly permeable preferential flow paths, where the solute particle's trajectory can certainly follow the streamlines [*Baeumer et al*., 2014]. An extension of the standard vector fADE can therefore be practically important, as will be discussed further in the following.

This study proposes an MIM physical model to address the above numerical challenges and capture the transient anomalous diffusion with mixed retention and early arrivals in natural heterogeneous media. The resulting 3-D anomalous transport simulator provides a flexible modeling platform that captures both early arrivals and retention. To answer the first challenge, a general memory function which defines the particle waiting time distribution [*Haggerty et al*., 2000; *Schumer et al*., 2003a; *Benson and Meerschaert*, 2009] will be considered, where (1) the MIM mass exchange rate can have any number and weight (as suggested by *Haggerty et al*. [2000] and demonstrated by others [*Feehley et al*., 2000; *Dean and Reimus*, 2008]), and (2) the tempered stable density used by *Meerschaert et al*. [2008] is selected as a specific and useful form of the memory function. The tempered stable density was also recommended by *Cvetkovic* [2011] as a universal model for hydrological transport; see further discussion below. To answer the second challenge mentioned above, the concurrent fast displacement of particles along streamlines will be incorporated for mobile solutes using the subordination technique proposed recently by *Baeumer et al*. [2009, 2014]. The novelty of this paper is that we incorporate both MIM and streamline-oriented fast jumps, to capture both retention and fast-moving effects. Both are seen in applications, and neither one alone can reproduce both the late time retention and early arrivals seen in real data.

We will then focus on a fully particle-tracking based, Lagrangian interpretation of the resultant physical model. The Lagrangian solver is selected because it not only provides an efficient method to approximate the partial differential equations that govern the transport of solutes, but also describes directly the dynamics of the underlying physical process; see the extensive review in *Delay et al*. [2005] and *Salamon et al*. [2006]. For reactive tracer transport, the fully Lagrangian approach can also be superior to the classical continuum modeling approach in capturing mixing-controlled reaction kinetics [*Benson and Meerschaert*, 2008]. The Lagrangian solver can also be computationally efficient, since (1) the particles remaining in the immobile state will not waste any computation [*Zhang et al*., 2008], and (2) the grid-free scheme provides subflow-grid resolution of the simulated concentration without increasing the computational burden. In addition, to the best of our knowledge, the phase transition probability (TP) approach developed by *Salamon et al*. [2006] is the only particle-tracking scheme quantifying the MIM mass exchange with multiple rate coefficients. The phase-transition probabilities combined with analytical expressions of plume spatial moments were previously proposed by *Michalak and Kitanidis* [2000] to quantify kinetic sorption with a new random-walk particle-tracking method (see their Figure 4 for a flow chart for the Lagrangian scheme). The TP at each time step, which defines the particle status (i.e., mobile or immobile), is the time-dependent particle mass which can only be calculated by approximating an exponential matrix [*Salamon et al*., 2006]. We will propose and evaluate various new Lagrangian approaches that directly track the dynamics of particles, where the TP and exponential matrix are not needed and therefore the particle-tracking scheme can be simplified. It is also noteworthy that the multirate method provides efficient simulating of late-time tailing behavior in contaminant transport, and the technology developed by this study provides an easy approximation of the multirate method.

The rest of the paper is organized as follows. In section 2, the transport model for anomalous dispersion is shown by combining the mobile/immobile concept and subordination to regional flow. In section 3, we develop a two-step Lagrangian solver to approximate the physical model for retention, early arrivals, and their mixture, based on the renewal-reward process. The resultant particle-tracking solutions are then validated against other approaches available for simple cases. In section 4, the Lagrangian solver is applied to model anomalous dispersion in multidimensional heterogeneous porous and fractured media. The applicability of the new model is checked using numerical data and field and laboratory measurements. In section 5, we discuss future extensions of the Lagrangian framework for transient flow and nonstationary regional-scale media. Conclusions are finally drawn in section 6.

Note that this study focuses on the implementation of the Lagrangian solver, and therefore the theoretical analysis of nonlocal transport and behavior are shown only in appendices. For example, Appendix A reviews nonlocal transport models, which underpins the model development in this study. Mechanism and detection of early arrivals are discussed in Appendix D, to explain further the early arrivals found in applications in section 4.

2. Time and Space Nonlocal Transport Models

Previous time and space nonlocal transport models are reviewed in Appendix A. Successful applications of the multirate mass transfer (MRMT) model and the time fADE model motivate us to use both multiple rates and the temporally tempered stable density to capture retention due to mass exchange, where the latter leads to the tempered stable fADE model proposed by *Meerschaert et al*. [2008]. In addition, we will add a specific space fractional-derivative term in the transport process to characterize spatial nonlocality, resulting in a fractional-derivative model that can characterize complex anomalous transport including the mixed retention and early arrivals. It is also noteworthy that although the time fADE is selected in this study, nonlocality in time has been extensively studied by various researchers, including those reviewed in Appendix A.

To build the physical model, we first consider the fast-motion component in solute transport. *Baeumer et al*. [2014] proposed the following model to capture super-diffusion along flow lines using subordination:

$$\frac{\partial C}{\partial t} = -\nabla_{\vec{v}}\, C + \sigma(\nabla_{\vec{v}})^{\alpha}\, C + \nabla[D(\vec{x},t)\nabla C]\,, \tag{1}$$

where C $[ML^{-3}]$ denotes the solute concentration; $\vec{v}$ $[LT^{-1}]$ is the velocity vector; σ [dimensionless] is a scalar factor; $1 < \alpha < 2$ [dimensionless] is the order of the space fractional derivative; and $D(\vec{x},t)$ $[L^2T^{-1}]$ is the diffusion coefficient. The advection operator $\nabla_{\vec{v}}$ is defined via $\nabla_{\vec{v}}\, C = \nabla(\vec{v}\, C)$. The solution of (1) with $D = 0$ can be obtained by specifically transforming the solution to the ballistic equation $\partial C/\partial t = -\nabla(\vec{v}C)$ (see Appendix B). This transformation is known as subordination [*Baeumer et al*., 2001; *Schumer et al*., 2003a; *Sokolov and Metzler*, 2004] and can capture mechanical dispersion due to the local variation from the mean velocity; see *Baeumer et al*. [2014] for a detailed explanation.

Previous studies developed three other approaches based on the fractional engine to describe apparent (such as power-law distributed) early arrivals. First, *Baeumer et al*. [2001] used the fractional power (with an index less than one of the classical advection-dispersion operator $-\nabla(\vec{v}) + \nabla[D(\vec{x},t)\nabla]$, to add additional displacement for the mass center. Second, *Meerschaert et al*. [2001] and *Schumer et al*. [2003b] proposed a multiscaling, vector fADE to capture super-diffusive particle trajectories deviating from streamlines. Third, *Meerschaert et al*. [2010] used a γ-stable waiting time process with index $1 < \gamma < 2$ to describe continuous jumps. All the three approaches can efficiently capture rapid dynamics, but they do not directly describe mechanical dispersion following streamlines. Therefore we select model (1) for this study.

Next we extend (1) to capture the concurrent retention due to mobile/immobile mass exchange. The total solute concentration consists of two parts:

$$C_{tot} = \theta_m C_m + \theta_{im} C_{im}, \tag{2}$$

where C_{tot}, C_m and C_{im} $[ML^{-3}]$ denote the solute concentration in the total, mobile, and immobile phases, respectively; and θ_m and θ_{im} [dimensionless] are the porosity in the mobile and immobile phases, respectively.

Following the mobile/immobile formulation procedure outlined in *Schumer et al*. [2003a], we obtain an MIM model describing mixed retention and early arrivals:

$$\frac{1}{\theta_m}\frac{\partial C_{tot}}{\partial t}=\frac{\partial C_m}{\partial t}+\beta\frac{\partial C_m}{\partial t}*f(t)=-\nabla_{\vec{v}}\,C_m+\sigma(\nabla_{\vec{v}})^{\alpha,\lambda_L}C_m+\nabla[D(\vec{x},t)\nabla C_m]\,, \tag{3a}$$

$$C_{im}(\vec{x},t)=\int_0^t f(t-s)\,C_m(\vec{x},s)\,ds\,, \tag{3b}$$

where $f(t)$ $[T^{-\gamma}]$ is a general memory function defining the distribution of rate coefficient for mass exchange between the mobile and parallel immobile blocks; β $[T^{\gamma-1}]$ is the total capacity coefficient; and λ_L $[L^{-1}]$ is the tempering parameter in space.

Model (3a) shows that the total concentration change is due to the advective flux $\nabla_{\vec{v}}\,C_m$, the subordinated mechanical dispersive flux $\sigma(\nabla_{\vec{v}})^{\alpha,\lambda_L}C_m$, and the molecular diffusive flux $\nabla[D(\vec{x},t)\nabla C_m]$ in the mobile phase, since particles embedded in the immobile phase cannot move. Model (3b) implies that the immobile phase concentration is related to the previous mobile concentration (at the same location) filtered by the memory function. We assume that the immobile phase is clean of tracers initially, to represent the typical contamination observed in the field. If the immobile concentration is not zero initially, the decay of the initial immobile mass needs to be added to the right-hand side of (3b).

Given the form of the memory function $f(t)$, model (3) can be finalized. This study considers two commonly used $f(t)$. First, *Haggerty et al*. [2000] showed that in most cases, $f(t)$ defines multiple (N) rate coefficients (ω_j) with arbitrary weights:

$$f(t)=\sum_{j=1}^{N}\omega_j\,b(\omega_j)\,e^{-\omega_j t}\,, \tag{4}$$

where $b(\omega_j)$ is the probability mass function of first-order rate coefficients. Inserting (4) into (3), we obtain the following MRMT model subordinated to regional flow:

$$\frac{\partial C_m}{\partial t}+\sum_{j=1}^{N}\beta_j\frac{\partial C_{im}^j}{\partial t}=-\nabla_{\vec{v}}\,C_m+\sigma\,(\nabla_{\vec{v}})^{\alpha,\lambda_L}C_m+\nabla[D(\vec{x},t)\nabla C_m]\,, \tag{5a}$$

$$\frac{\partial C_{im}^j(\vec{x},t)}{\partial t}=\omega_j\left[C_m(\vec{x},t)-C_{im}^j(\vec{x},t)\right],\quad \text{where } j=1,2,\ldots,N\,. \tag{5b}$$

It is noteworthy that when N is large or even approaching infinity, then the memory function (4) needs to be truncated and the application of model (5) may not be convenient. This challenge motivates us to consider a second memory function.

Second, for a truncated power-law function $f(t)$ [*Meerschaert et al*., 2008]:

$$f(t)=\int_t^{\infty}e^{-\lambda_T r}\,\frac{\gamma\,r^{-\gamma-1}}{\Gamma(1-\gamma)}\,dr\,, \tag{6}$$

the MIM model (3) becomes

$$\frac{\partial C_m}{\partial t}+\beta e^{-\lambda_T t}\frac{\partial^{\gamma}\left[e^{\lambda_T t}C_m\right]}{\partial t^{\gamma}}=-\nabla_{\vec{v}}\,C_m+\sigma\,(\nabla_{\vec{v}})^{\alpha,\lambda_L}C_m+\nabla[D(\vec{x},t)\nabla C_m]\,, \tag{7a}$$

$$\frac{\partial C_{im}}{\partial t}=e^{-\lambda_T t}\,\frac{\partial^{\gamma}\left[e^{\lambda_T t}C_m\right]}{\partial t^{\gamma}}\,, \tag{7b}$$

where λ_T $[T^{-1}]$ is the truncation parameter in time, and the time index $0<\gamma<1$. Model (7) is a time tempered fADE subordinated to regional flow. If $\sigma=0$, then (7) reduces to the model of *Cvetkovic* [2011]. Note that model (7) is a specific case of model (5) with an infinite number of mass exchange rate coefficients that have an exponentially truncated power-law pdf. Hence the time fractional ADE is a specific MRMT model, and the MIM model proposed above (i.e., (3) and (7)) considers also early arrivals due to spatial nonlocality using a fractional spatial derivative. This (exponentially truncated) fractional spatial derivative leads to a special operator in the nonlocal dispersive constitutive theory [*Cushman et al*., 1994], where the local variation

of solute concentrations is due to a weighted average of mechanical dispersive flux at upgradient zones. This weight, as defined by the memory function in the nonlocal dispersive constitutive theory [*Cushman and Ginn*, 2000], declines as an exponentially truncated power-law function in space. A physical interpretation for the standard fractional spatial derivative was also provided by *Schumer et al*. [2001] and *Molz et al*. [2002].

The above MIM models (5) and (7) will be solved using a Lagrangian approach in the next section. We will call (5) "the MRMT model," and (7) "the fractional MIM model."

3. Development of the Lagrangian Solver

3.1. Literature Review: The Renewal-Reward Process and the Corresponding Two-Step Lagrangian Solver

The renewal-reward process (RRP) is a classical model from probability theory that generalizes the Poisson process by allowing for holding times and jumping sizes [*Cinlar*, 1969; *Ross*, 1983; *Tijms*, 2003]. A stochastic process consisting of a random inter-renewal time between two random jumps can be regarded as a specific RRP. The CTRW framework reviewed by *Berkowitz et al*. [2006] therefore is a specific RRP; however, not every RRPs (where inter-renewal times and rewards can have various densities) including the one developed below should follow the same CTRW framework. Most importantly, time nonlocal models including the CTRW framework in hydrology and the MRMT model usually model retention and they do not handle early arrivals. Other RRPs have also been used to capture hydrological processes [*Kendall and Dracup*, 1992; *Fisher et al*., 2010].

The two-step random walk scheme (jump followed by waiting) embedded in the RRP had been used by various researchers. For example, a two-step Lagrangian solver was proposed by *Dentz and Berkowitz* [2003] to approximate the MRMT model, see also equations (13) and (14) in *Dentz et al*. [2004] and the brief description of methodology by *Berkowitz and Scher* [1998]. A two-step, fully Lagrangian scheme was applied by *Le Borgne and Gouze* [2008, equation (8)] (with continuous dispersion coefficient and the solution for the total phase), and was extended by *Le Borgne et al*. [2008, equation (1)] to describe non-Markovian transport. *Benson and Meerschaert* [2009] also proposed a random walk solution for an arbitrary immobile time density embedded in the MRMT model. *Edery et al*. [2009, 2010] developed a reactive, continuous time random walk particle-tracking model to quantify chemical kinetics due to non-Fickian transport. The above successful applications motivated us to select a similar two-step scheme. In the following we develop particle-tracking schemes in time (defining the renewal process J) and space (defining the rewards Y) that can be used to describe anomalous diffusion. The following Lagrangian scheme is new and simple, because it can explicitly model multiple first-order trapping processes, and early arrivals along streamlines.

3.2. An Explicit Two-Step Lagrangian Solver and Renewal-Reward Process

The Lagrangian solver contains two major steps to model particle dynamics. The first step is to assign the mobile and immobile times for each particle during each jump. This step corresponds to the renewal process in the RRP; see for example, *Meerschaert and Scheffler* [2008]. The horizontal axis in Figure 1a shows the holding time J_n $[T]$ (representing the clock/physical time) for a random walker after the n-th jump:

$$J_n = \sum_{i=1}^{n} dt_i = \sum_{i=1}^{n} (dM_i + dI_i)\,, \tag{8}$$

where $n = 1, 2, \ldots, L$; and dt_i is the i-th holding time consisting of the mobile (or operational) time dM_i and the immobile waiting time dI_i (Figure 1b).

In the second step, we calculate the trajectory of random-walking particles. The corresponding cumulative reward (representing the particle position at the clock time t) is

$$Y_t = \sum_{i=1}^{X_t} dx_i\ . \tag{9}$$

Here dx_i $[L]$ denotes the i-th jump size during the mobile time dM_i, and X_t [dimensionless] denotes the number of jumps that have occurred by the clock time t:

$$X_t = \sum_{n=1}^{\infty} \Pi_{J_n \le t} = \sup\{n : J_n \le t\} \ , \tag{10}$$

where Π is the indicator function, and X_t is a nonzero integer (i.e., the maximum number of n satisfying $J_n \le t$).

3.3. Step 1: Renewal Processes for Retention

The core of the renewal process is to efficiently assign the MIM time. In natural geological media, the strong physical and chemical heterogeneity can cause complex mass transitions, where the number of mass exchange rates (representing the number of immobile zones with different sorption/trapping capabilities) can be either finite (such as model (5)) or infinite (such as model (7)) [*Haggerty et al.*, 2000]. The Lagrangian scheme needs to be adjusted for the two cases, to achieve the most computational efficiency.

3.3.1. Renewal Process for the MRMT Model (5)

When there are a finite number (N) of immobile zones, each solute particle can transition between the mobile state and the N immobile states, with the forward mass exchange rate $\omega_j \beta_j$ and the reverse rate ω_j for the j-th MIM pair (Figure 1b). In this study, the immobile zones are assumed to be parallel, so there is no direct mass exchange between immobile zones. Here we propose and compare two different methods to generate the mobile time dM. The following Lagrangian scheme can also be revised conveniently to account for other initial conditions. For example, if a particle starts at one specific immobile state, then its initial state number is known, providing the immobile time dI directly.

3.3.1.1. Method 1: Mobile Time Follows a Single-Rate Exponential Distribution

This method treats the mobile time dM as a random variable and the mobile phase as a single state. To do this, we combine all the N pairs of mobile/immobile states and build the following exponential distribution (Figure 1b) with an overall rate parameter A:

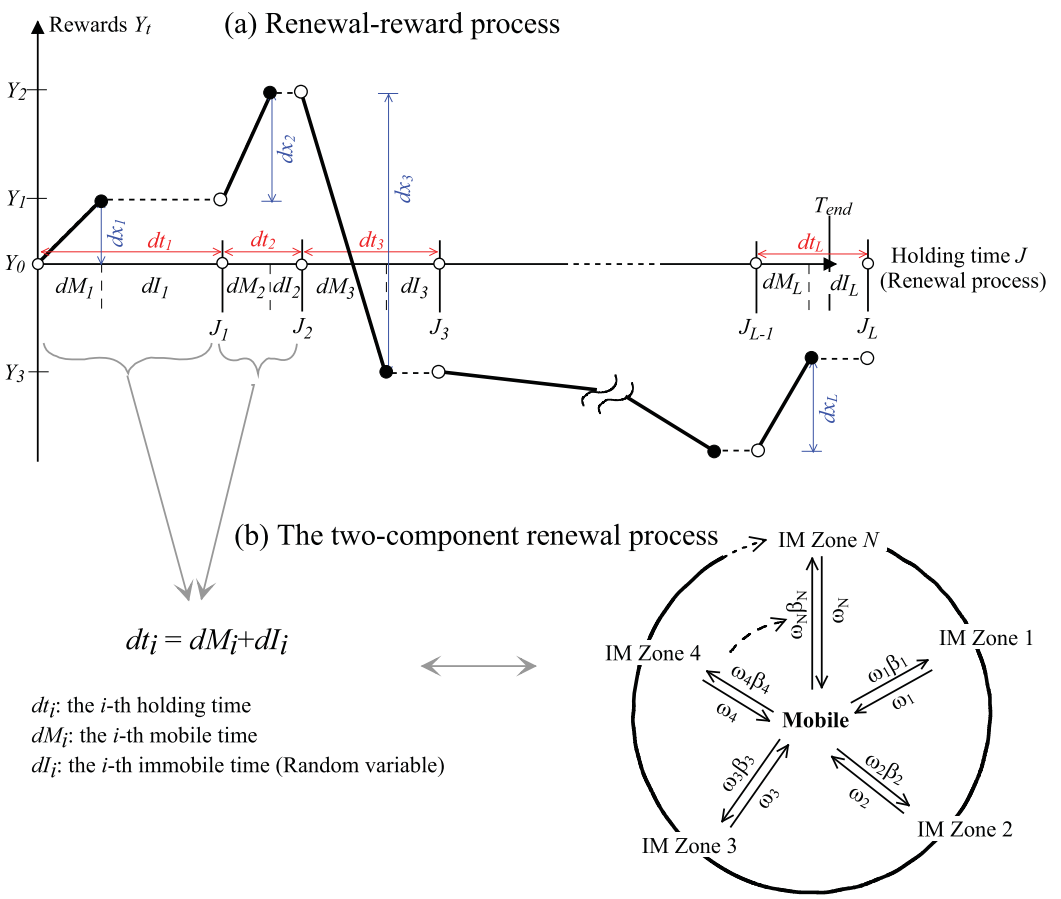

Figure 1. (a) The renewal-reward process (RRP): the holding time and the rewards. (b) A two-component, multistate Markov renewal process ($dt_i = dM_i + dI_i$, where $i = 1, 2, \cdots L$) to illustrate the motion (advection and dispersion) of a particle in time. In the legend, "IM" denotes IMmobile.

$$A=\sum_{j=1}^{N}\omega_j\beta_j\,. \tag{11}$$

The mobile time at the *i*-th jump, dM_i, is an exponentially distributed random variable with the pdf $P(t)=A\,e^{-At}$:

$$dM_i=\frac{\ln(1-U^{\circ})}{-A}\,, \tag{12}$$

where U° is a uniform random number in $(0,\,1)$.

The corresponding immobile state can then be determined by the relative contribution of the corresponding mobile state. The probability for a particle to enter the *k*-th immobile state is proportional to the inverse of the mean mobile time (which is $\omega_k\beta_k$) in the corresponding *k*-th mobile state. This motivates us to use the normalized mean mobile time, $\omega_k\beta_k/A$, to define the probability for the particle reaching the *k*-th immobile state. A uniform $(0,\,1)$ random number $U^{\star}$ is therefore generated to identify the corresponding immobile state *k*:

$$\sum_{j=1}^{k-1}\frac{\omega_j\beta_j}{A}<U^{\star}\le\sum_{j=1}^{k}\frac{\omega_j\beta_j}{A}\,. \tag{13}$$

After *k* is defined by (13), the corresponding waiting time dI_i can then be calculated by

$$dI_i=\frac{\ln(1-U_k)}{-\omega_k}\,, \tag{14}$$

where the uniform $(0,\,1)$ random number U_k is independent of the previously generated U° in (12). See *Ross* [1983] for details.

The above scheme can be validated using two known facts. First, when $N=1$ and $\alpha=2$, the MRMT model (5) reduces to the well-known single-rate mobile/immobile model [*Haggerty et al.*, 2000]. In this simplified case, the mobile time *dM* and the immobile time *dI* generated above have the exponential pdf

$$P(dM)=\omega\beta\,e^{-\omega\beta\,dM}\,, \tag{15a}$$

$$P(dI)=\omega\,e^{-\omega\,dI}\,, \tag{15b}$$

which is consistent with the known particle-tracking scheme [*Benson and Meerschaert*, 2009]. The mobile time pdf (15a) follows the known conclusion that the conventional ADE is the scaling limit of a CTRW with a Poisson distribution for motion times and Gaussian distribution for jump sizes [*Metzler and Klafter*, 2000].

Second, the above numerical scheme captures the ratio between the mean mobile and immobile times. The mean mobile time T_m calculated by the above method is

$$T_m=\frac{1}{A}\,. \tag{16}$$

The immobile time generated by the above method follows the Hyper-exponential distribution with the pdf

$$P(t)=\sum_{i=1}^{N}\left[\omega_i\,e^{-\omega_i t}\right]\frac{\omega_i\beta_i}{A}\,, \tag{17}$$

where p_i denotes the proportion of each exponential function in the Hyper-exponential distribution. The mean immobile time T_{im} therefore is

$$T_{im}=\sum_{i=1}^{N}\frac{\beta_i}{A}=\frac{\beta_{\mathrm{tot}}}{A}\,, \tag{18}$$

where β_{tot} [dimensionless] is the total capacity coefficient representing the ratio of mass in all immobile states to mass in the mobile domain at equilibrium [*Haggerty et al.*, 2000]. The ratio between the mean immobile time and the mean mobile time should also equal β_{tot}, since the mean residence time also defines the mass of particles remaining in the state at equilibrium. Equations (16) and (18) lead to the ratio $T_{im}/T_m=\beta_{\mathrm{tot}}$, showing that the above Lagrangian scheme produces the correct ratio between mean mobile and immobile times.

3.3.1.2. Method 2: A Constant, Mean Random Mobile Time

In the above method, the mobile time dM is exponentially distributed. A constant dM may be favored for some applications (due to its simplicity and its potential in increasing the computational efficiency), motivating the development of Method 2.

First, we can define the constant dM as the mean mobile time T_m (16):

$$dM_i = T_m = \frac{1}{A}\,. \tag{19}$$

The immobile time dI_i can be calculated the same as (13), where both methods generate the same mean mobile time (16). Their mean immobile times are also the same (i.e., (18)). This method can be applicable for a transport time much longer than the mean mobile time.

Then the mobile time

$$dM_i = \Delta t = T_m\,. \tag{20}$$

Note that the renewal theorem is the basis for this approximation. For any renewal process, the number X_t of jumps by time t in equation (9) is related to the jump rate β by $X_t/\beta \to 1$ as t goes to infinity. That is, X_t is approximately βt and the approximation gets better as t increases. The subsequent random immobile time dI can be generated by

$$dI_i = \frac{\ln(1-U)}{-\omega_k}\,A\,\Delta t\,, \tag{21}$$

where the state k is evaluated by (13), and the resultant mean immobile time is $T_{im} = \Delta t\,\beta_{\mathrm{tot}}$. This scheme may require a longer transport time than the above one to reach a reliable asymptotic solution.

All the above Lagrangian schemes will be validated in Sec. 3.3.3.

3.3.2. Renewal Process for the Fractional MIM Model (7)

The time-domain Langevin approach proposed by *Zhang et al.* [2008] separates time into a linear mobile portion and a stable random noise representing the immobile portion. The same approach can be extended to the tempered stable model [*Meerschaert et al.*, 2008]. The mobile time dM is now a user defined time step (which can be either constant or time dependent), and the immobile time dI_i is a conditionally tempered stable random noise rescaled by dM and β:

$$dI_i = \left[\cos\left(\frac{\pi\gamma}{2}\right)\beta\,dM\right]^{1/\gamma} dL_{\gamma,\lambda_T}(\beta^\star = +1,\ \sigma^\star = 1,\ \mu = 0)\,. \tag{22}$$

Here dL_{γ,λ_T} [dimensionless] denotes a tempered stable random variable with the truncation parameter λ_T, the maximum skewness $\beta^\star$, unit scale $\sigma^\star$, and zero shift μ.

An alternative method could also be developed based on *Benson and Meerschaert* [2009], where the mobile time distributes exponentially. We select the first method, due to the flexibility of dM. Validations of this method combined with the reward process will be shown in section 4.

3.3.3. Numerical Validations

To test the above Lagrangian scheme developed for the renewal process, here we limit the reward process to be the one-dimensional traditional ADE with a constant velocity V and dispersion coefficient D. This simplifies the MRMT model (5) as:

$$\frac{\partial C_m}{\partial t} + \sum_{j=1}^{N}\beta_j\frac{\partial C_{im}^j}{\partial t} = -V\frac{\partial C_m}{\partial x} + D\frac{\partial^2 C_m}{\partial x^2}\,, \tag{23a}$$

$$\frac{\partial C_{im}^j(\vec{x},t)}{\partial t} = \omega_j\left[C_m(\vec{x},t) - C_{im}^j(\vec{x},t)\right],\quad j = 1,2,\ldots,N\,. \tag{23b}$$

We first check the applicability of the above Lagrangian method for model (23) with a single mass exchange rate. A few numerical examples are shown in Figure 2. The simulated tracer snapshots and breakthrough curves (BTCs) match well the numerical solutions using the transition probability or TP method proposed by *Salamon et al.* [2006]. Note that the RRP based Lagrangian method is computationally more efficient than the TP method, since the former accounts explicitly for the immobile phase in the renewal process (so that less

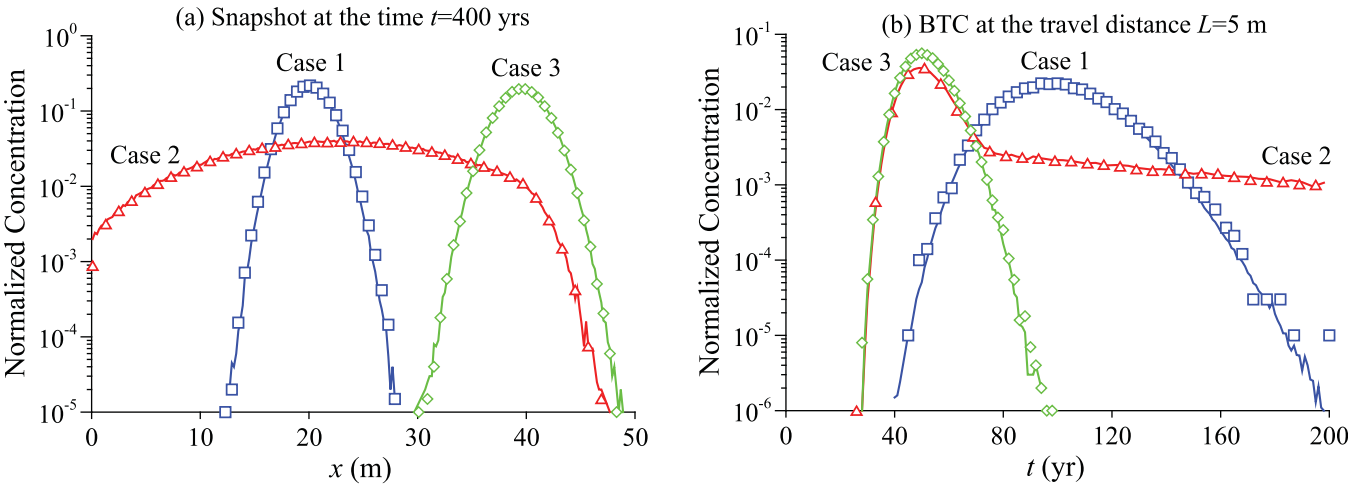

Figure 2. The simplified MRMT model (23) with a single mass exchange rate: the simulated (a) tracer snapshots and (b) BTCs using *Salamon et al.*'s [2006] transition probability approach (symbols) and our Method 1 (lines). In Case 1, model parameters are as follows: rate coefficient $\omega = 1$ year^{-1}, and capacity coefficient $\beta = 1$. In Case 2, ω=0.01 year^{-1} and $\beta = 1$. In Case 3, $\omega = 1$ year^{-1} and β=0.01. The other model parameters are as follows: $V = 0.1$ m/yr, $D = 0.005$ m^2/yr, and $\theta_{im}/\theta_m = \beta$. Here θ_{im} (denoting the immobile zone porosity) and θ_m (i.e., porosity of the mobile zone) were used by *Salamon et al.* [2006] to control the capacity coefficient β.

operations are needed). In addition, the TP method needs to approximate an exponential matrix (by truncating the corresponding Taylor series), which is not needed for the Lagrangian method developed by this study.

Results for the simplified MRMT model (23) with $N > 1$ using Method 1 are shown in Figure 3. A multirate series of spherical diffusions are considered, where the rate coefficient $\omega_i = i^2\pi^2\varepsilon$ (where i=1, 2, . . . 8, and ε =0.00432 day^{-1} is the diffusion rate coefficient for spherical diffusion [*Haggerty et al.*, 2000]), and capacity coefficient $\beta_i = \frac{6}{i^2\pi^2}\beta_{tot}$ (where $\beta_{tot} = \frac{\theta_{im}R_{im}}{\theta_m R_m}$ is the total capacity coefficient).

Methods 1 and 2 are then used to solve the above numerical model. Results (Figure 4) show that Method 1 matches the "true" solution slightly better than Method 2 does, as expected.

3.4. Step 2: Rewards for the Concurrent Early Arrivals

Early arrivals can occur concurrently with retention for contaminant transport in natural geological media. Fast displacement along streamlines due to mechanical dispersion can be captured efficiently using the subordination to regional flow, a method proposed by *Baeumer et al.* [2014].

Following step 1 developed in section 3.3, we first assign the mobile and immobile times:

$$t_i = t_{i-1} + dM_i + dI_i\,, \tag{24}$$

where t_i $[T]$ denotes the clock time at the i-th jump, and the two times dM_i and dI_i can be calculated by the two methods discussed in section 3.3.

We then calculate the displacement of particles during the mobile time dM_i. It contains two components. The first displacement due to advection and molecular diffusion can be calculated using the traditional particle-tracking scheme [*LaBolle et al.*, 1996, 1998]. The second displacement due to mechanical dispersion can be calculated by:

$$\delta S_i = \vec{v}\,\delta t_i\,, \tag{25}$$

if the velocity $\vec{v}$ remains constant in space. Here $\vec{v}$ is defined as the velocity at the position of the particle at the end of the last jump. If $\vec{v}$ varies in space, each component of the space-dependent velocity vector can be approximated by Darcy's law:

$$\vec{v}_i(\vec{x}) = -\theta^{-1}(\vec{x})\sum_{j=1}^{3}\bar{K}_{ij}(\vec{x})\,\nabla_j h(\vec{x}),\quad i=1,2,3$$

where h is the hydraulic head, θ is the local porosity, and $\bar{K}_{ij}$ is the ij-th component of the hydraulic conductivity tensor. The hydraulic head h can be computed by solving the saturated groundwater flow equations [*Harbaugh*, 2005], and, in some cases, approximated from monitoring data (see further discussion in the next

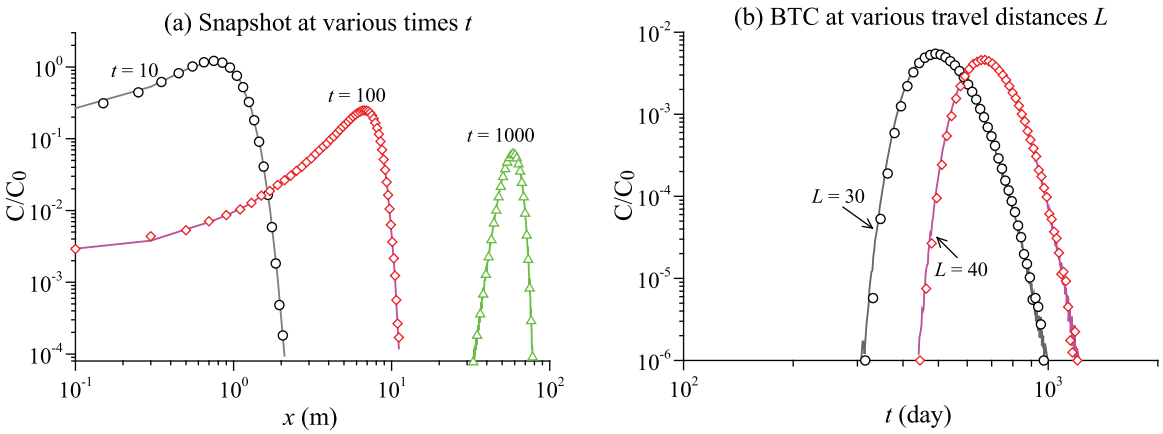

Figure 3. The simplified MRMT model (23) with multiple mass exchange rates ($N = 8$): the simulated (a) tracer snapshots and (b) BTCs using *Salamon et al.*'s [2006] transition probability approach (symbols) and Method 1 (lines). The eight rate and capacity coefficients are shown in the text. The other model parameters are: $V = 0.0864$ m/d, $D = 0.00432$ m^2/d, $\theta_m = 0.2$, and $\theta_{im} = 0.1$, which are the same as those used by *Salamon et al.* [2006]. In Figures 3a and 3b, the length dimensions are meters, and the time dimensions are days.

section). In this case, the travel distance can be approximated by the predictor-corrector method, or the semi-analytical method assuming a linear interpolation of velocities within each grid [*LaBolle et al.*, 1996, 1998]. The operational time for subordination δt_i $[T]$ in (25) is a conditionally tempered stable random variable scaled by the mobile time dM_i (similar to (22)):

$$\delta t_i = \left[-\cos\left(\frac{\pi\alpha}{2}\right)\sigma\, dM_i\right]^{1/\alpha} dL_{\alpha,\lambda_L}(\beta^* = +1,\ \sigma^* = 1,\ \mu = 0)\,. \tag{26}$$

Here dL_{α,λ_L} [dimensionless] denotes a tempered α-stable random variable.

For validation purposes, we apply the above Lagrangian solver for a one-dimensional transport model (without molecular diffusion) where the other numerical method can be developed. Here the F-MIM model (7) reduces to

$$\frac{\partial C_m}{\partial t} + \beta e^{-\lambda_T t}\frac{\partial^\gamma\left[e^{\lambda_T t}C_m\right]}{\partial t^\gamma} = -V\frac{\partial C_m}{\partial x} + \left[\sigma V^\alpha\right]e^{-\lambda_L x}\frac{\partial^\alpha\left[e^{\lambda_L x}C_m\right]}{\partial x^\alpha}\,, \tag{27a}$$

$$\frac{\partial C_{im}}{\partial t} = e^{-\lambda_T t}\frac{\partial^\gamma\left[e^{\lambda_T t}C_m\right]}{\partial t^\gamma}\,, \tag{27b}$$

where V $[LT^{-1}]$ is the 1-D constant velocity. For cross-verification, we developed the implicit Eulerian finite difference method to solve equation (27). Some numerical examples are shown in Figure 5, where the Lagrangian solutions generally match the Eulerian solutions. Figure 5 shows the influence of α on leading fronts of tracer plumes, as expected.

To draw a conclusion, in the renewal process, a (random or constant) mobile time is generated to explicitly account for the multiple first-order mass exchange, in additional to the random immobile time. This process interprets the physical process of mass exchange: a mobile particle can be trapped by one immobile domain along its trajectory. In the subsequent reward process, the particle experiences advection and molecular diffusion. An additional lateral displacement is then calculated to account for mechanical dispersion along streamlines, which can be Fickian if the medium is homogeneous or non-Fickian if the medium is strongly heterogeneous. Therefore, the physical model and Lagrangian solver characterize nonlocal transport in both time and space. A detailed physical interpretation of super-diffusion on streamlines can be found in *Baeumer et al.* [2014].

4. Applications: Capturing Anomalous Diffusion in Multidimensional Porous and Fractured Media

Here we apply the above solver to capture anomalous diffusion observed in multidimensional, heterogeneous porous or fractured media (except for Case 5 which is a 1-D leaching process), where our two-step Lagrangian approach is the only viable solver.

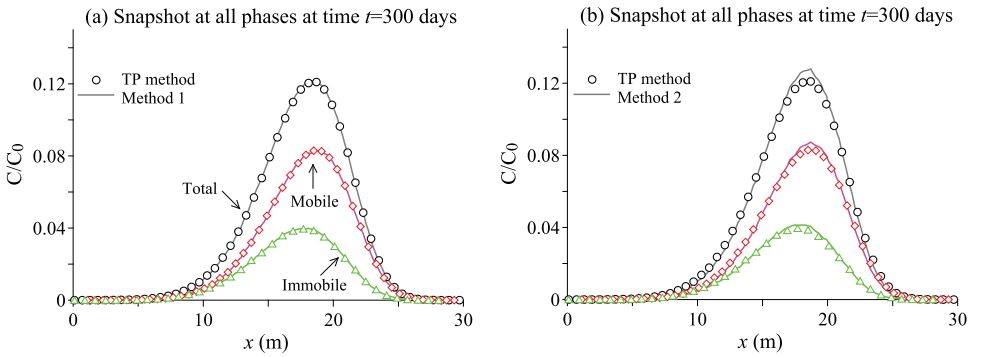

Figure 4. The simplified MRMT model (23) with multiple mass exchange rates ($N = 8$): the simulated tracer snapshots at all phases using the transition probability method (symbols), (a) Method 1 (lines) and (b) Method 2 (lines). The model parameters are the same as those used in Figure 3.

4.1. Case 1: Anomalous Transport in a 2-D Heterogeneous Porous Medium

One of the motivations of this study is to build an efficient solver to capture spatiotemporally nonlocal transport conditioned on local aquifer properties. Natural heterogeneous porous media usually exhibit multiscale physical and/or chemical heterogeneity. Geophysical and/or hydrogeological information typically can be incorporated into the numerical model. It is therefore desirable to combine non-Fickian transport and aquifer information available at relevant scales. Models (5) and (7) provide such a tool by introducing the local variation of flow properties in nonlocal transport models.

For example, Figures 6–8 show retention and fast jumps of solute particles through a two-dimensional heterogeneous aquifer with both divergent and convergent flow zones. Figure 6a shows the flow model (with a uniform cell size 2 m $\times$ 2 m), and Figure 6b shows the steady state flow field calculated by MODFLOW [*Harbaugh*, 2005] and the resultant streamlines calculated by the Lagrangian solver developed above.

Figure 7 compares the simulated plume assuming different immobile properties (i.e., different renewal processes), while the reward process is assumed to be the classical ADE. In Figure 7a, the Lagrangian solver is used to calculate the particle plume where the transport follows the classical ADE (i.e., Fickian diffusion). Figure 7b shows the plume for the MRMT model (5) with a single rate of mass exchange, where the spatial distribution of the particle plume is relatively limited compared to Figure 7a. In Figure 7c, strong retention is modeled (where the renewal process is described by the F-MIM model (7)), where the sequestration near the source is apparent.

Figure 8 shows the mixed retention and early arrivals, which is the Lagrangian solution of the F-MIM model (7). While retention traps solute mass around the source area, early arrivals along streamlines exhibits a leading edge toward the pumping well. The leading edge in the streamlines model can be more realistic in fractured aquifers, as implied by model comparisons at the Shoal test site (see Case 3, section 4.3). Comparison of Figure 8a and Figure 8b shows that, with the decrease of the space index α and an increase of the scalar factor σ (representing larger jumps along streamlines), the leading edge of particle plumes becomes heavier.

4.2. Case 2: Upscaling Retention Observed in 3-D Alluvial Aquifers Represented by High-Resolution Hydrofacies Models

4.2.1. Capturing Anomalous Transport in Alluvial Settings

Alluvial settings typically exhibit complex geometric structures and intrinsic heterogeneity. In particular, the high-permeability ancient channel deposits that tend to be interconnected in 3-D space may form preferential flow paths [*Fogg et al.*, 2000], while the surrounding low-permeability floodplain layers retard transport by trapping a significant amount of solute mass [*LaBolle and Fogg*, 2001]. Following the Markov chain based geostatistic methods used by *LaBolle and Fogg* [2001], here we built high-resolution hydrofacies models to represent 3-D alluvial aquifers, with one realization shown in Figure 9a. One hundred different but equally possible realizations were generated, and the ensemble average of plumes (calculated by the same methodology shown in *LaBolle and Fogg* [2001] and then projected to the horizontal plane) is shown in Figures 9b–9d. The resultant plumes will be used as "measurements" to check the applicability of the physical model and its Lagrangian solver developed by this study. The "measured" plumes exhibit sequestration

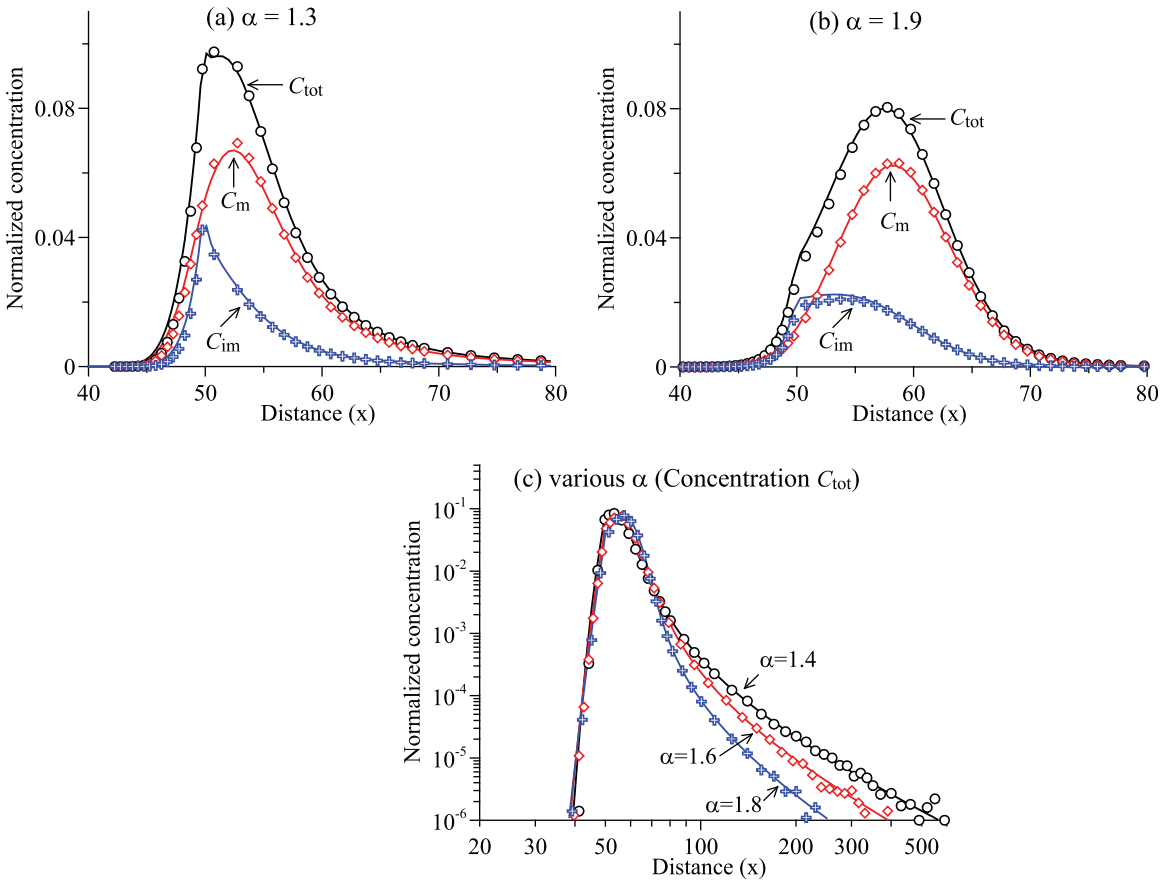

Figure 5. The combined retention and early arrivals described by the simplified F-MIM model (27): Lagrangian solutions (symbols) versus the implicit finite different solutions (lines) of tracer snapshots at time $t = 10$. The modeled concentration for particles at the total, mobile, and immobile phases for (a) α=1.3 and (b) α=1.9, respectively. (c) The modeled concentration at the total phase for α=1.4, 1.6, and 1.8, respectively. The other model parameters are as follows: γ=0.5, β=0.1, λ_T=0.001, velocity $v = 1$, the scale factor $\sigma = 1$, and porosity 1. The initial instantaneous point source is located at $x = 50$.

behavior (i.e., a significant amount of solute mass remains near the initial source location), one of the typical characters of retention (Figures 9b–9d).

Model parameters in (7) were either predicted or fitted (Table 1). Parameters defining the renewal process, including γ, β, and λ_T, were estimated given medium heterogeneity using the method proposed in *Zhang et al.* [2014b]. The space-independent index γ (which controls the power-law slope of the concentration

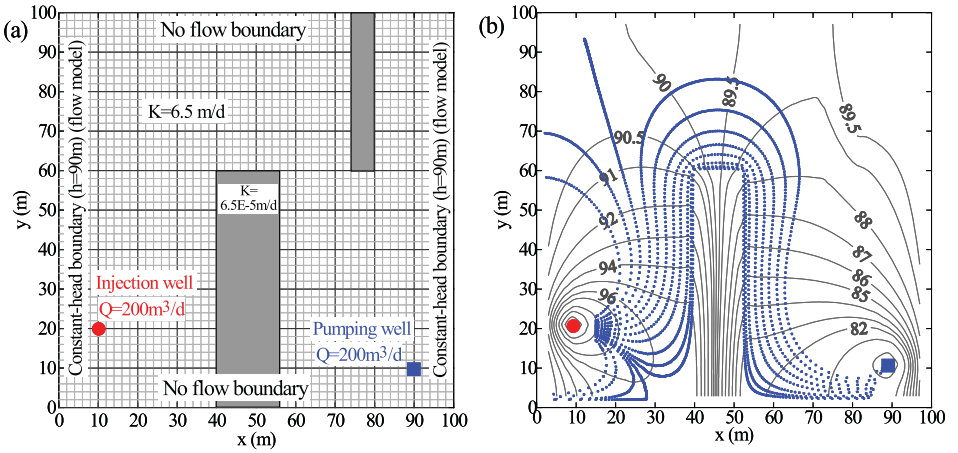

Figure 6. Application 1: (a) The 2-D flow model. (b) The calculated steady state flow field (grey lines are the contour map of the simulated hydraulic head (meter)) and the streamlines (blue dotted lines).

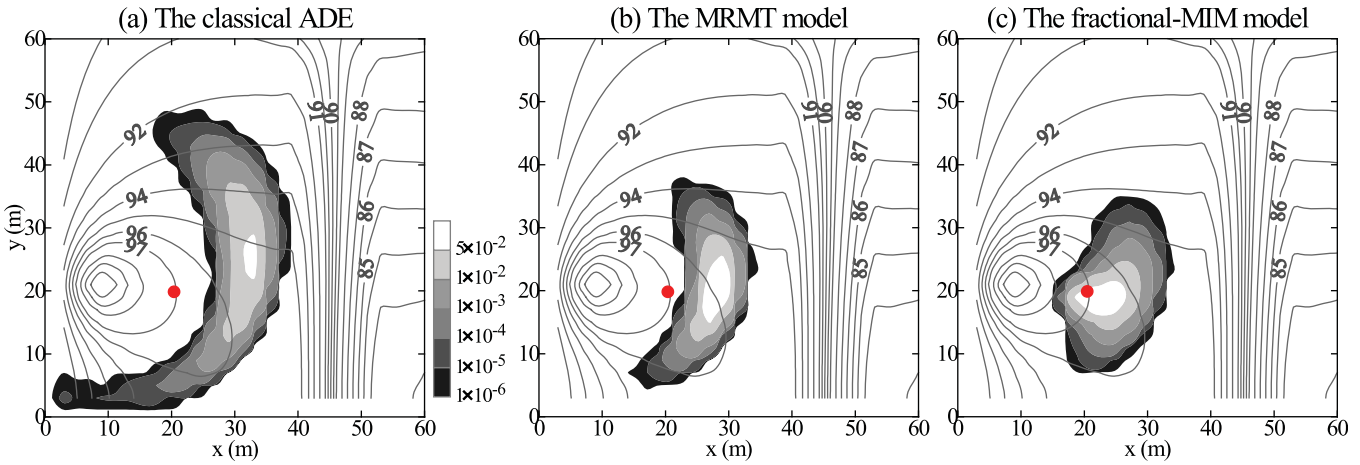

Figure 7. Application 1: The simulated 2-D plume distribution at time $t = 600$ days for (a) the (a)classical ADE model, (b) the MRMT model (5) with a single mass exchange rate and $\alpha = 2$, and (c) the F-MIM model (7) with $\alpha = 2$ using the Lagrangian solver. The legend shows the normalized concentration. The red dot denotes the location of the initial instantaneous point source at $x = 20$ m and $y = 20$ m, and porosity is 0.3. Two million particles were released initially. In the MRMT model (5) (Figure 7b), the rate coefficient ω=1.0 day^{-1} and the capacity coefficient β=1.0. In the F-MIM model (7) (Figure 7c), the time index γ=0.5, the fractional capacity coefficient β=0.2 day$^{-0.5}$, and the time truncation parameter λ_T=1×10^{-8} day^{-1}.

profile) and the temporal truncation parameter λ_T (which captures the rate of transition for preasymptotic transport) can be predicted given the volume fraction of low-permeability deposits classified by thickness. For example, λ_T can be predicted by $D^*/(Z^*)^2$, where D^* is the molecular diffusion coefficient used in the Monte Carlo simulations and Z^* is the effective thickness of the fine-grained layer. The capacity coefficient β (which distinguishes the status of solute particles) can be predicted as the ratio between the mean residence time (for particles in relatively low-permeable layers) and the mean advective time [*Benson and Meerschaert*, 2009]. Details of the prediction and hydrogeological interpretation of the above parameters can be found in *Zhang et al.* [2014b]. The mean velocity along the longitudinal direction (V_x) can be predicted by the arithmetic mean of local velocities [*Zhang et al.*, 2007a], while the mean velocity along the transverse direction (V_y) was assumed to be zero. The other parameters, including the ones controlling the reward process, were fitted using the observed plume distribution shown in Figures 9b–9d. In particular, the truncation parameter λ_L controls the decline rate of the leading front, the space index α captures the power-law section of the leading front, and the scalar factor σ describes the overall shape of the plume front. The best-fit λ_L is relatively large, to characterize the quick decline of the concentration at the plume front.

Fitting results show that the Lagrangian approximation of the F-MIM model (7) can generally capture the overall trend of the multidimensional plume in all phases (Figures 9e–9g), although the Monte Carlo simulations contain apparent noises near especially the leading edge. The computational approach developed by this study therefore may provide a tool for upscaling complex transport in alluvial settings.

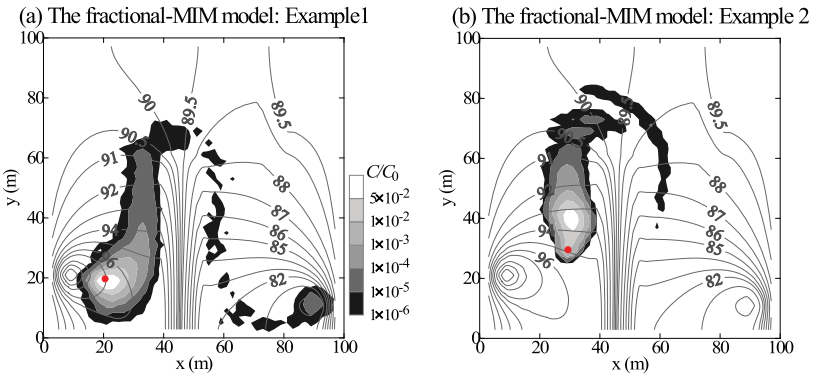

Figure 8. Application 1: The 2-D plume distribution at time $t = 400$ days for the F-MIM model (7) with different parameters. The red dot denotes the initial point source. (a) Model parameters: γ=0.5, β=0.2 day$^{-0.5}$, λ_T=1×10^{-8} day^{-1}, α=1.50, λ_L=1×10^{-8} m^{-1}, and $\sigma = 2$. (b) Model parameters: γ=0.5, β=0.01 day$^{-0.5}$, λ_T=1×10^{-8} day^{-1}, α=1.70, λ_L=1×10^{-6} m^{-1}, and $\sigma = 1$.

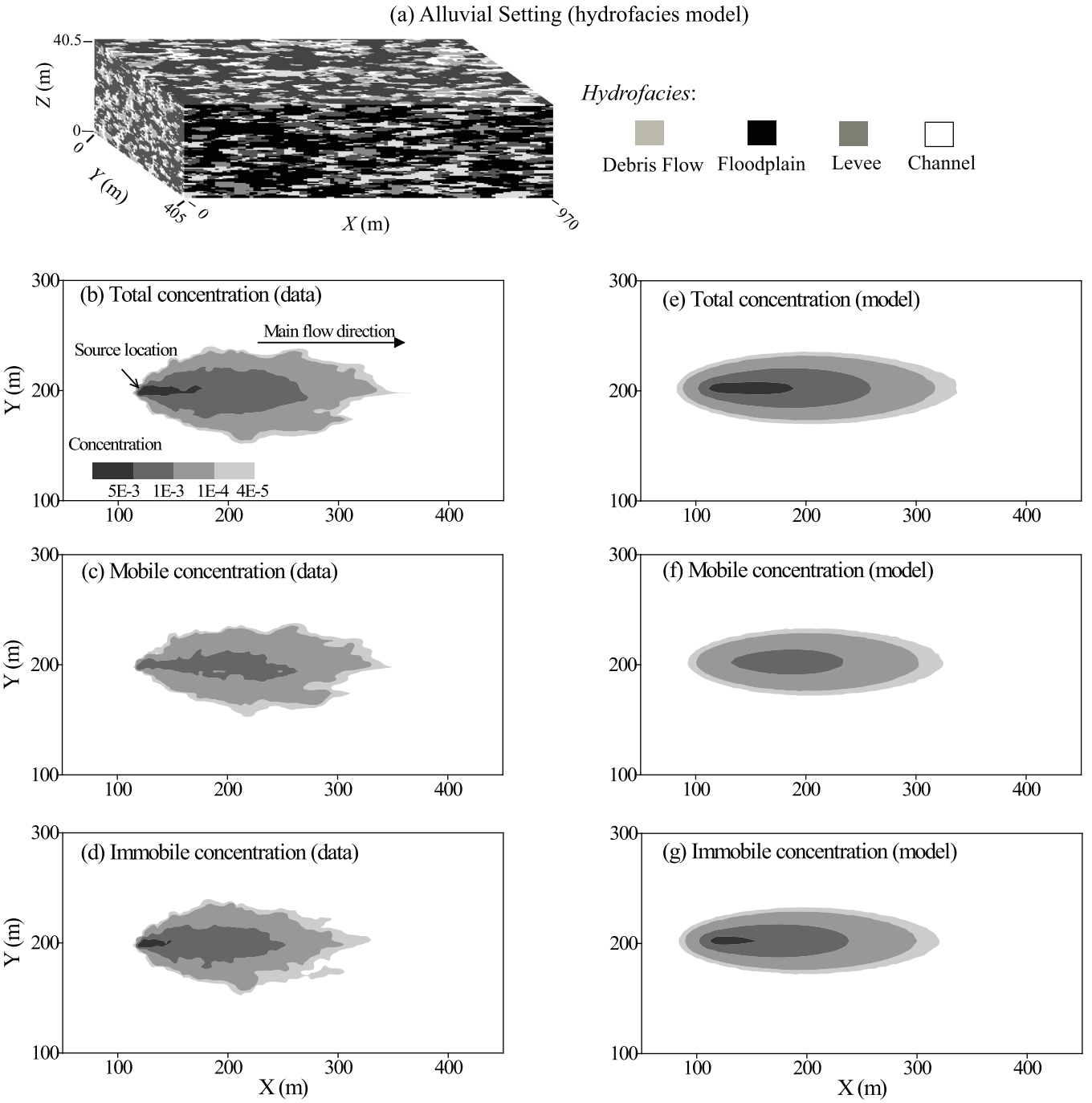

Figure 9. Application 2: 3-D view of one realization of (a) the hydrofacies model and (b–d) the 2-D plume distribution at time $t = 10$ years for the "measured data" (Monte Carlo simulations) versus (e–g) the best-fit using the F-MIM model (7). The model parameters are shown in Table 1.

4.2.2. Comparisons With Existing Models

We compare the F-MIM model (7) with existing time nonlocal transport models. First, the following time fADE (T-fADE) model is selected since it contains only one fitting parameter (i.e., the dispersion coefficient D):

$$\frac{\partial C_m}{\partial t} + \beta e^{-\lambda_T t} \frac{\partial^\gamma \left[e^{\lambda_T t} C_m \right]}{\partial t^\gamma} = -V \frac{\partial C_m}{\partial x} + D \frac{\partial^2 C_m}{\partial x^2}, \tag{28a}$$

Table 1. The Predicted and Fitted Parameters for the Alluvial Setting in Application 2[a]

Model	γ[b] Predicted	λ_T (1/year) Predicted	β (year$^{\gamma-1}$) Predicted	V_x (m/yr) Predicted	D (m^2/yr) Fitted	σ[b] Fitted	α[b] Fitted	λ_L (1/m) Fitted
F-MIM (7)	0.56	0.00237	0.63	14.6	10.0	0.60	1.76	0.25
T-fADE (28)	0.56	0.00237	0.63	14.6	115.0	N/A	N/A	N/A

[a]γ–Time Scale Index; λ_T–Space Truncation Parameter; β–Capacity Coefficient; V_x–Longitudinal Velocity; D–Diffusion Coefficient; σ–Scalar Factor; α–Space Scale Index; and λ_L–Tempering Parameter in Space.
[b]dimensionless.

$$\frac{\partial C_{im}}{\partial t} = e^{-\lambda_T t}\,\frac{\partial^{\gamma}\left[e^{\lambda_T t} C_m\right]}{\partial t^{\gamma}}, \tag{28b}$$

where the time nonlocal transport parameters β, λ_T and γ, and the mean velocity V can all be predicted using the methods discussed in section 4.2.1. As discussed in Appendix C, the time fADE (28) is also a specific MRMT model which was shown to be universal in capturing retention. To the best of our knowledge, here model (28) requires the least number of fitting parameters, compared with the other time nonlocal transport models reviewed in Appendix A. Predictability for model (28) may be extended for the other time nonlocal models. If model (28) cannot capture the retention process observed in this case (we emphasize here again that the time nonlocal models typically capture retention, not early arrivals; see our review in Appendix A), we will test further the other time nonlocal models.

Second, the single-rate mass transfer (SRMT) model was found to be efficient in capturing "cigar-shaped" contours of non-Gaussian transport in 2-D by *Uffink et al*. [2012]. Hence it is selected to compare with the F-MIM model (7).

Figures 10d–10f compares the three nonlocal transport models in capturing the longitudinal snapshots at various times. First, the F-MIM model (7) using parameters fitted in Figure 9 predicts not only the concentrations for solute at all phases (Figures 10a–10c), but also the strong sequestration and the leading plume edge at all times. Second, the time fADE model (28) captures the apparent retention, but it slightly underestimates the leading plume edge at most sampling cycles, although a large dispersivity ($\approx$ 8 m) is used. Third, the SRMT model underestimates the strong retention near the source, which is not a surprise because a single mass exchange rate does not represent the multiple mass exchange between the mobile zone and various immobile blocks [see also *Haggerty et al*., 2000]. It is also noteworthy that the leading plume edge is weak in this specific case, and therefore the time fADE model (28) can be a simplified alternative of the F-MIM model (7) at a large travel distance; see further discussion for the mechanism for early arrivals in Appendix D.

4.3. Case 3: Anomalous Transport in Fractured Media at the Shoal Test Site

4.3.1. Applicability of the F-MIM Model in a Coarse Flow Field

Fractures are common in geologic media and typically exhibit erratic heterogeneity [*Tsang and Neretnieks*, 1998; *Berkowitz*, 2002]. The resultant transport is usually anomalous. Here we check the applicability of the F-MIM model (7) and the Lagrangian solver developed above in capturing real-world anomalous diffusion observed in fractured rocks.

Tracers were injected and monitored in one fractured medium located at the SHOAL test site, Nevada [*Reimus et al*., 2003]. Groundwater flow can be simplified as a radial flow [*Benson et al*., 2004], which can be calculated by MODFLOW (Figure 11a).

In this case, all transport model parameters were fitted using the observed tracer BTCs, due to the lack of medium heterogeneity information. The early arrivals in the BTC are due to fast moving particles, which can be used to fit the parameters defining the reward process. For example, the space index α and the scalar parameter σ control the power-law slope of the early time BTC, while λ_L truncates this power-law increase of BTC. Hence the slope and the transition from power-law to exponential for the early time BTC were used to fit α, σ, and λ_L. The late-time tail of the BTC is due to retention, and hence it can be used to fit the parameters defining the renewal process (which are γ, β, and λ_L). In particular, γ controls the power-law slope of the late-time BTC, while β shifts the late-time BTC up and down (since it assigns the mass ratio of particles

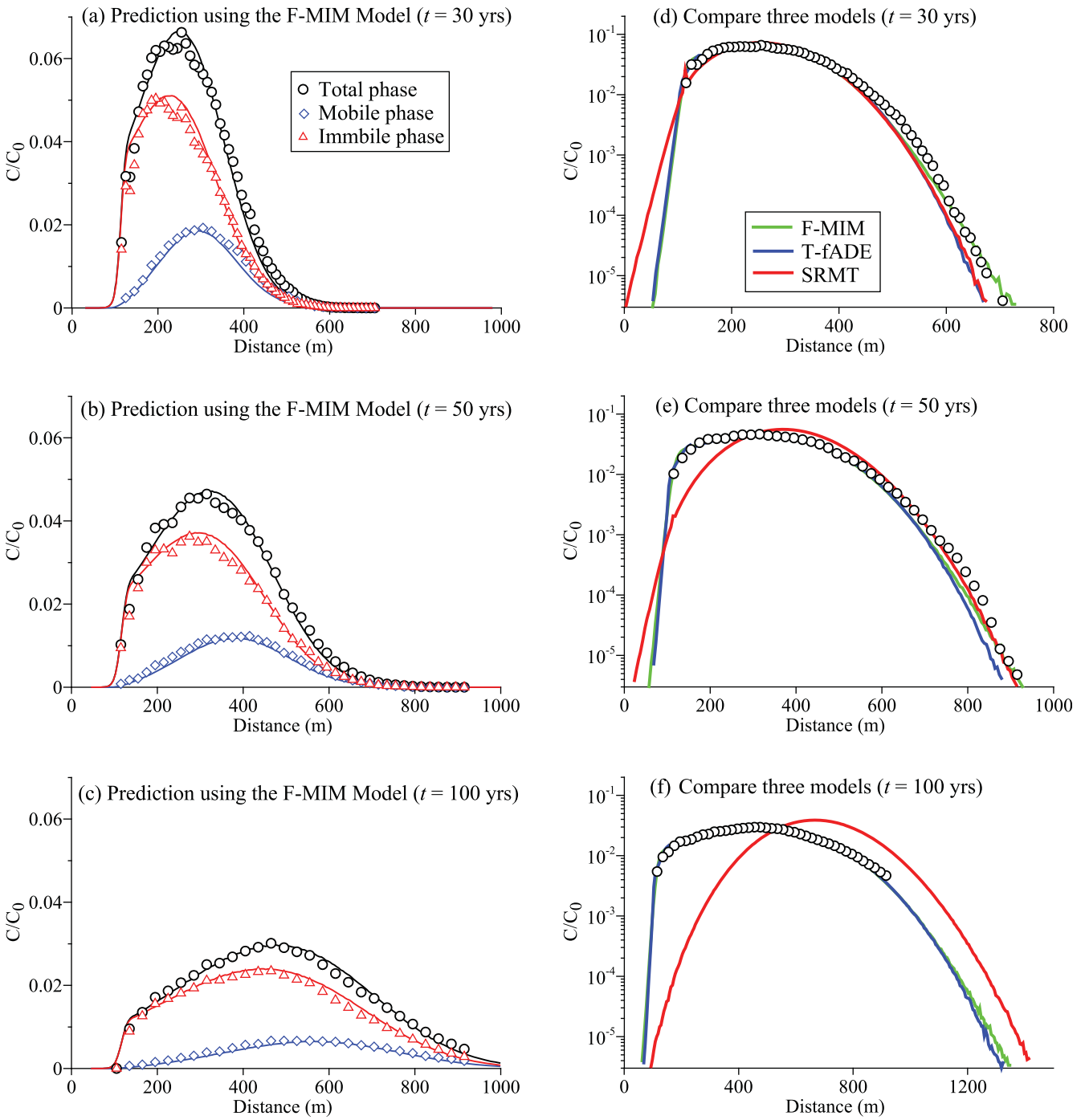

Figure 10. Application 2: Snapshots along the longitudinal direction at time t = (a) 30 years, (b) 50 years, and (c) 100 years, where the symbols are Monte Carlo simulations and the lines represent the F-MIM model (7) predictions. (d–f) Comparison of the three model solutions for the total (mobile plus immobile) concentration, where the symbol "F-MIM" denotes the fractional MIM model (7), "T-fADE" denotes the time fADE model (28), and "SRMT" denotes the single-rate mass transfer model. Parameters used for the F-MIM model and the T-fADE model are shown in Table 1. The best-fit rare coefficient for the SRMT model is ω=0.2 year^{-1}, and the predicted capacity coefficient β (0.63) has the same value as the other models.

in mobile and immobile phases). λ_T affects the transition for the late-time BTC from power-law to exponential. Due to the missing information of such transition, a small λ_T was selected (in other words, we ignored the possible transition behavior due to the lack of observation).

The resultant parameters of model (7) using the above fitting schemes for tracer Pentafluorobenzoate (PFBA) are shown in Table 2. The modeled PFBA plume is shown in Figure 11e. The simulated PFBA BTC generally matches the observation (Figures 11e and 11f). Note that the best-fit parameters for retention

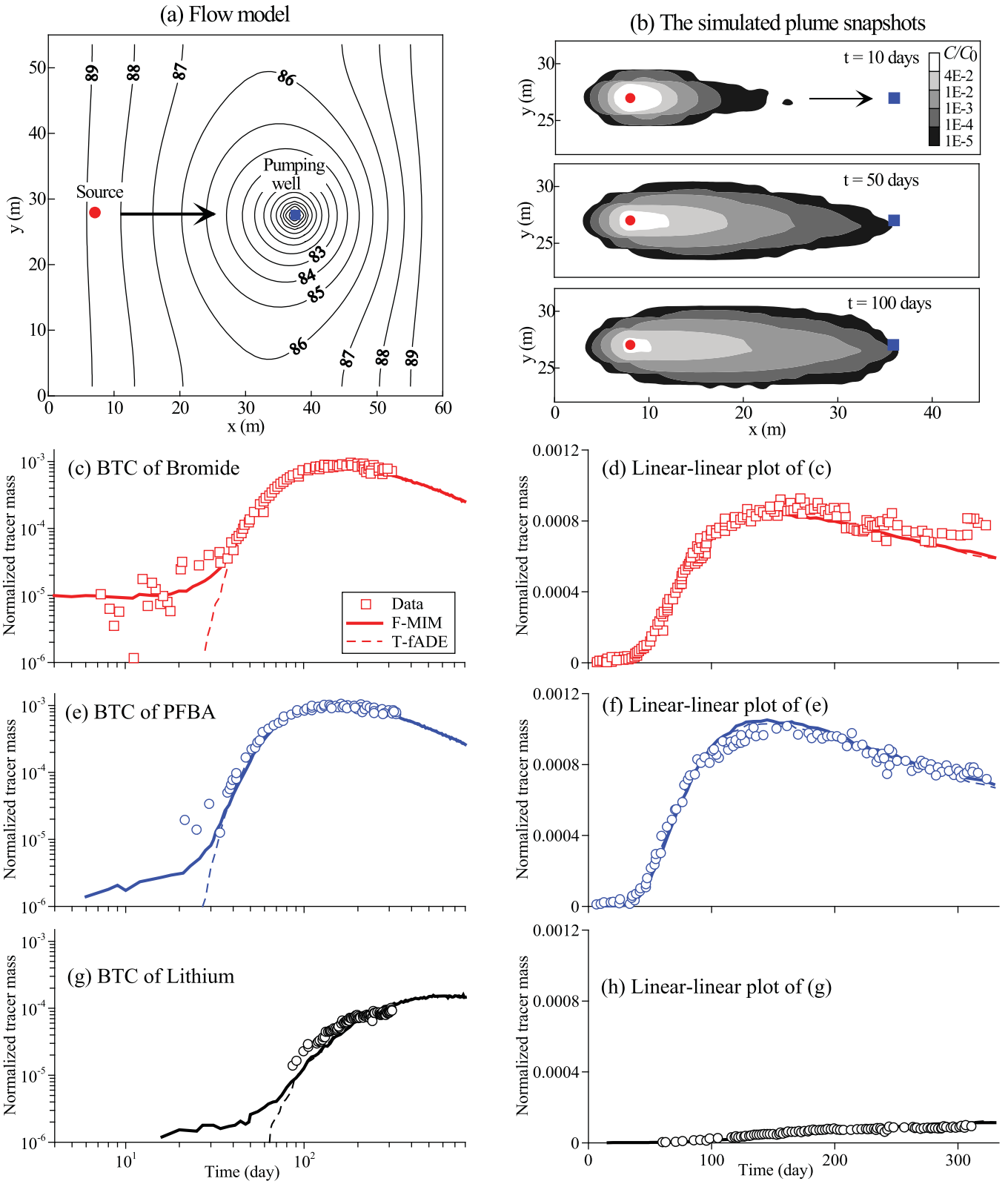

Figure 11. Application 3: (a) The 2-D flow model for the Shoal test site. (b) The simulated plume snapshots at various times using the F-MIM model (7). The red dot denotes the position of the initial point source, and the blue rectangle denotes the pumping well. (c) The measured Bromide breakthrough curves [*Reimus et al.*, 2003] (symbols) versus the best-fit BTCs (lines) using both the F-MIM (7) and the T-fADE (28). (d) The liner-linear plot of Figure 11c. (e and f) PFBA BTCs and (g and h) Lithium BTCs.

Table 2. The Predicted and Fitted Parameters for Tracer Transport at the Shoal Test Site in Application 3[a]

Tracer	γ[b]	λ_T (1/day)	β (day$^{\gamma-1}$)	D (m^2/yr)	σ[b]	α[b]	λ_L (1/m)
PFBA	0.46	1×10^{-8}	0.49	1×10^{-5}	1	1.95	0.03
Bromide	0.44	1×10^{-8}	0.48	1×10^{-5}	1	1.95	0.005
Lithium	0.44	1×10^{-8}	1.05	1×10^{-5}	1	1.95	0.02

[a]γ–Time Scale Index; λ_T–Space Truncation Parameter; β–Capacity Coefficient; D–Diffusion Coefficient; σ–Scalar Factor; α–Space Scale Index; and λ_L–Tempering Parameter in Space
[b]dimensionless.

(especially the time truncation parameter λ_T) contain high uncertainty due to the incomplete observation of the BTC tail. The Lagrangian solver of model (7) can also efficiently capture the observed BTCs for the other tracers (Bromide and Lithium) (Figure 11), by adjusting parameters λ_L, γ and β (note that the space index α and the scale parameter of subordination σ remain the same for all tracers, implying that the fracture probably causes similar fast motions for different tracer particles). The best-fit λ_L is the smallest for Bromide since the early time tail of the observed Bromide BTC is the heaviest (Figure 11c). The best-fit time index γ is similar for all three tracers, implying that γ relates more to the medium (especially the matrix) property than to the tracers themselves. The capacity coefficient β, however, differs between tracers, probably due to the different sorption capability for different chemicals (since β defines the mass ratio of particles in the immobile phase and the mobile phase).

4.3.2. Comparison With Existing Models

Further numerical experiments show that early arrivals of Bromide and PFBA in this fractured aquifer can not be captured by the T-fADE model (28) (Figure 11), implying that early arrivals along fractures can not be efficiently quantified by a time nonlocal transport model. In addition, although the late-time observations were missing in all tracer BTCs, the SRMT model (where the late-time BTC tail declines as fast as exponential) may not be able to capture the retention process observed in a typical fractured aquifer, where regional-scale matrix diffusion tends to enhance the late-time tailing. It is also noteworthy that the observed BTC for Lithium does not show early arrivals, probably due to a relatively high detection limit of Lithium.

4.4. Case 4: Mixed Retention and Early Arrivals in Fractures

Here we analyze anomalous transport in fractured media with different scales and well-controlled properties, to compensate the fractured aquifer in Case 3 with limited information. First, Monte Carlo simulations of conservative solute transport through random two-dimensional, regional-scale discrete fracture networks (DFN) conducted by *Reeves et al.* [2008a, 2008b] exhibit strong retention combined with apparent fast jumps along streamlines (i.e., fractures). The DFNs were generated according to fracture statistics obtained from field studies that describe fracture length, transmissivity, density, and orientation (see Figure 12a for one example). *Reeves et al.* [2008a, 2008b] found that the leading edge of the plume (representing the largest particle jumps or early arrivals) contains an upper truncation that violates the assumption of the classical Lévy motion model,

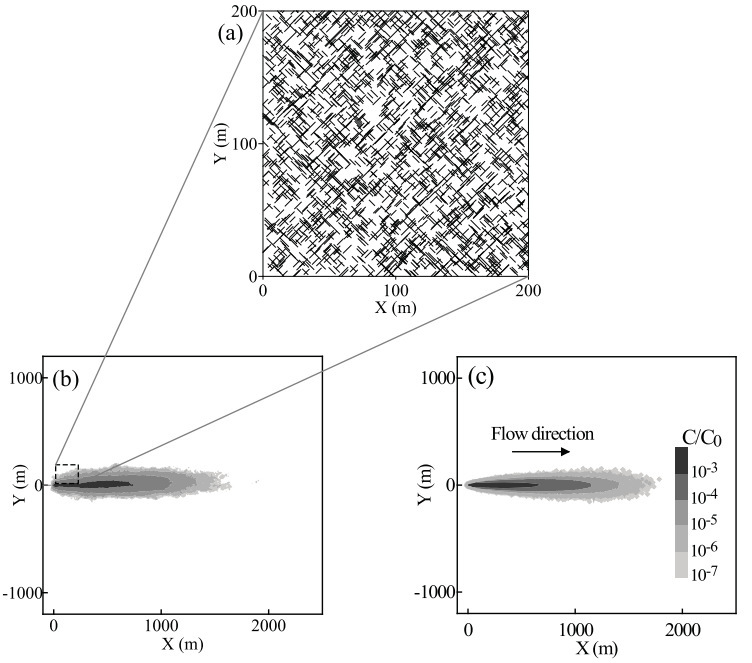

Figure 12. Application 4a: (a) Discrete fracture network. (b) Ensemble particle plume at time $t=1000$ years. (c) Best-fit using the F-MIM model (7).

Table 3. The Predicted and Fitted Parameters for Tracer Transport in DFN in Application 4a[a]

Model	γ[b]	λ_T (1/year)	β (year$^{\gamma-1}$)	V_x (m/yr)	D (m^2/yr)	σ[b]	α[b]	λ_L (1/m)
F-MIM (7)	0.38 Predicted	1×10^{-5} Predicted	0.07 Predicted	1.9 Fitted	1.0 Fitted	0.9 Fitted	1.80 Fitted	0.06 Fitted

[a]γ–Time Scale Index; λ_T–Space Truncation Parameter; β–Capacity Coefficient; V_x–Longitudinal Velocity; D–Diffusion Coefficient; σ–Scalar Factor; α–Space Scale Index; and λ_L–Tempering Parameter in Space.
[b]dimensionless.

motivating the application of the F-MIM model (7) with a tempered stable density. Results show that model (7) with a coarse flow field (i.e., an uniform velocity along the longitudinal direction) can characterize the skewed plume (Figure 12c). Model parameters are shown in Table 3. For a better visualization in model comparisons, we further quantify transport along a single fracture below.

Second, transport of tracers through small scale ($<$ 100 cm), single empty fractures were measured in the laboratory by *Chen et al.* [2011] and *Qian et al.* [2011]. All the measured BTCs exhibit heavy late-time tails (see e.g., Figure 13), which might be due to mass exchange between the boundary layer near the fracture wall and the mobile domain near the plane of symmetry [*Qian et al.*, 2011]. Numerical experiments show that the T-fADE model (28) captures the slow decline of the BTC at late times, but it significantly underestimates the early arrivals. The F-MIM model (7) does simulate both the early and late time tails in the BTC, because it explicitly models fast displacement in fractures. Model parameters are shown in Table 4. The heavy-tailed early arrivals in the BTC imply that there is no apparent truncation for large jumps, and therefore we can predict a small space truncation parameter λ_L (1.0×10^{-5} m^{-1}) for this case.

Therefore, our results improve on *Cvetkovic* [2011], showing that while his tempered power law time-nonlocal framework does seem to be a universal framework for capturing retention phenomena, it is also necessary to employ a space-nonlocal framework such as the F-MIM model (7) to capture the concurrent early arrivals.

4.5. Case 5: Model Application for Multiple First-Order Trapping Events

We check the developed implementation for multiple first-order trapping events in Arsenic leaching from saturated soils. Many column transport experiments revealed that the desorption of As(V), which is the thermodynamically stable redox state under oxidizing conditions in soils, may follow multiple rates including both fast reaction and long-term kinetics. For example, *Fuller et al.* [1993] fount that a period of rapid ($<$ 5 min) As(V) uptake from solution was followed by continued uptake for at least 8 days. *O'Reilly et al.* [2001] found that $>$35% of the sorbed As can be released rapidly within 24 h, and it took more than 5 months to 1 year to remove the remaining As. Similar multiple-rate kinetics were also observed by other researchers, and here we apply model (23) to capture arsenic dynamics in soils documented in *Qi and Donahoe* [2011].

Qi and Donahoe [2011] performed column leaching experiments on arsenic-contaminated soil samples. The measured BTC shows rapid initial arsenic release, followed by a prolonged tailing which declines linearly in

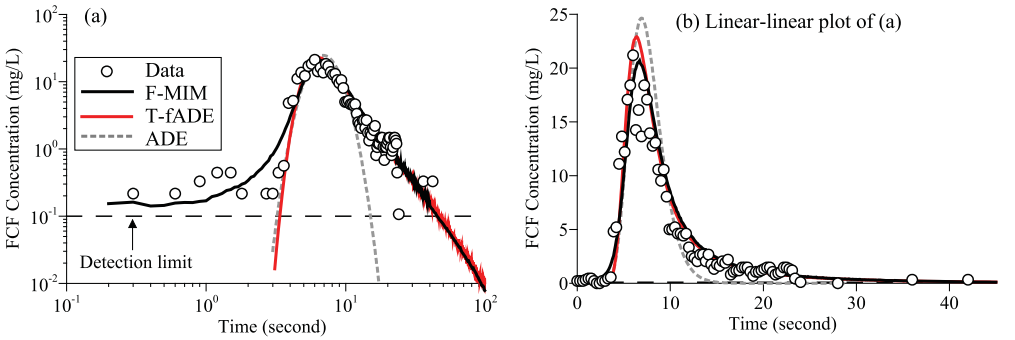

Figure 13. Application 4b: (a) 1-D BTC of Brilliant Blue CFC through a single parallel plane fracture with the length of 25.5 cm. (b) The linear-linear plot of Figure 13a. In this experiment, the fracture aperture is 0.0073 m, and the average flow rate is 0.055 m/s. See Table 4 for model parameters.

Table 4. The Predicted and Fitted Parameters for Tracer Transport in a Single Fracture in Application 4b[a]

Model	γ[b]	λ_T (1/s)	β ($s^{\gamma-1}$)	V_x (m/s)	D (m^2/s)	σ[b]	α[b]	λ_L (1/m)
F-MIM (7)	0.65	0.02	0.53	0.055	N/A	0.08	1.75	1.0×10^{-5}
	Fitted	Fitted	Fitted	Measured	N/A	Fitted	Fitted	Predicted
T-fADE (28)	0.65	0.02	0.53	0.055	0.016	N/A	N/A	N/A
	Fitted	Fitted	Fitted	Measured	Fitted	N/A	N/A	N/A

[a]γ–Time Scale Index; λ_T–Space Truncation Parameter; β–Capacity Coefficient; V_x–Longitudinal Velocity; D–Diffusion Coefficient; σ–Scalar Factor; α–Space Scale Index; and λ_L–Tempering Parameter in Space. In the legend, "s" means second.
[b]dimensionless.

a semi-log plot although the measurements contain strong noises (Figure 14b). We first quantify the leaching experiment using the SRMT model with a relatively large rate coefficient ω (0.5 day^{-1}, representing a small mean residence time $1/\omega=2$ days), which generates a fast release of As and captures the early peak. The late-time tail of the BTC is missed, as expected, implying a multiple-rate mass transfer process. We then apply the MRMT model (23) with two different rates to capture the general trend of the measured BTC, including both the early peak and the late-time tail of the BTC (Figure 14). Model parameters are shown in Table 5. In the MRMT model (23), the first rate is the same as the SRMT model which captures the fast peak. The second rate coefficient (0.02 day^{-1}) is much smaller, resulting in a long mean residence time and therefore capturing the late-time tail.

5. Discussion: Future Extension of the Lagrangian Solver

We first discuss the mechanism and detection of early arrivals in geological media in the literature and the above applications in Appendix D. We then discuss possible extensions of the Lagrangian solver for complex conditions.

5.1. Time-Dependent Velocity *v* and Diffusion Coefficient *D*

The time-dependent velocity can be calculated by separating the time into multiple stress periods, where the flow in each stress period is assumed to be steady state. When crossing the interfacial time (between two stress periods), the particle is either mobile or immobile. The immobile particle will remain immobile without changing the immobile time, if the time nonlocal transport parameters γ and β are time-independent. For the mobile particle, the original mobile time dM needs to be separated into two portions (dM_1 and dM_2) according to the interfacial time. The advective and diffusive displacement in each time portion can then be calculated by the velocity field in the corresponding stress period. Because v and D are defined in real time, the reward process with variable velocity (and dispersion coefficient) can be calculated conveniently.

5.2. Space-Dependent Time Index γ and Capacity Coefficient β

For a nonstationary alluvial setting, the variation of depositional environment can result in an apparent change in the spatial distribution of floodplain deposits, which may require space-dependent $\gamma(x)$ and $\beta(x)$ to characterize retention [*Zhang et al.*, 2007b]. To account for the impact of $\gamma(x)$ and $\beta(x)$ on particle

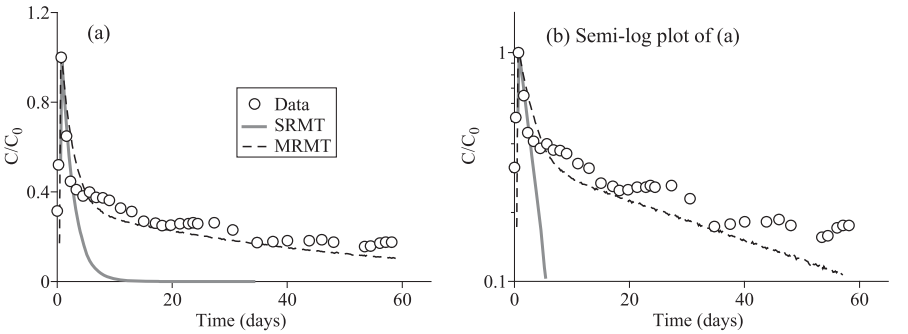

Figure 14. Application 5: (a) Comparison between the measured (symbols) and modeled (lines) As breakthrough curve using both the SRMT model and the MRMT model (23). Model parameters are shown in Table 5. (b) The semilog plot of Figure 14a, to show the late-time tail.

Table 5. Parameters for the SRMT Model and the MRMT Model (23) Used in Application 5[a]

Source	L (cm) Measured	V (cm/d) Measured	D (cm^2/d) Fitted	β_1[b] Fitted	ω_1 (1/day) Fitted	β_2[b] Fitted	ω_2 (1/day) Fitted
SRMT	40.64	100.9	0.001	0.5	0.5	N/A	N/A
MRMT	40.64	100.9	0.001	0.5	0.5	0.5	0.02

[a]L–the Travel Distance; V–Flow Velocity; D–Diffusion Coefficient; ω_j–Rate Coefficient; and β_j–Capacity Coefficient.
[b]dimensionless.

dynamics, we can generate a space-dependent random immobile time dI_i using (22), where the parameters γ and β are now spatial functions. Particle displacement during the mobile time dM should not be affected, if the mobile phase property does not change in space. Only when the particle finishes its moving and then transfers to the immobile state, will the impact of space-dependent retention capability be felt by the particle.

In addition, if γ and β change in time (due to for example the strong transient flow), the fractional-derivative model will contain a variable-order index. Depending on the definition of the variable index operator, one may either treat each random immobile time as an independent step during each jump (so that the random immobile time dI_i generator (22) is still valid) to describe a process that the previous index does not affect the next one, or quantify the influence (i.e., the memory impact) of the previous index by splitting the clock time according to the transient flow. We will test the extension proposed above in a future study.

6. Conclusions

This study is aimed at combing MRMT and fractional-derivative models and developing a general numerical solver in order to quantify the anomalous dynamics for tracers transport in multidimensional geological media. Anomalous transport can be incorporated into 2-D/3-D models with irregular flow fields. Both the mobile-immobile mass exchange mechanism and the preferential flow path are considered for tracer transport. Numerical development and model applications reveal five major conclusions.

First, the standard fractional-derivative models can be revised by (1) incorporating the multirate mass transfer process with a general memory function, and (2) allowing additional displacement along streamlines (representing mechanical dispersion deviating from the mean velocity in heterogeneous flow fields; see *Baeumer et al.* [2014] for details) whose distribution follows the tempered stable.

Second, an explicit two-step Lagrangian solver based on the renewal-reward process can approximate the above physical model, providing a numerical tool to capture anomalous dispersion for solutes in both space and time. The first step is the renewal process which defines retention for solute particles due to mass transfer between the mobile zone and any number of parallel immobile zones. The second step is the reward process that describes particle jumps in the mobile time, where a subordination to regional flow is applied to describe transient multidimensional fast jumps.

Third, to track particle dynamics in the time domain, the mobile time component of the renewal process can be calculated as either an exponential random variable or a preassigned time step, and the subsequent random immobile time follows a Hyper-exponential distribution for finite immobile zones or a tempered stable distribution for infinite zones with a specific, truncated power-law memory function.

Fourth, both numerical experiments and applications show that the generalized physical model and its fully Lagrangian solver can efficiently capture subgrid heterogeneity and flow variation, and therefore combine anomalous transport and aquifer information at various scales. In particular, leading edges of plumes and early arrivals of tracer BTCs are identified for transport in both regional-scale alluvial aquifers and fractured media at various scales. In column transport experiments, however, early arrivals in the mobile time may not be formed, due likely to the lack of long-range connectivity in flow between the upstream and the local region.

Fifth, this study shows that retention and early arrivals can be simulated as independent processes with different parameters in a physical model. In particular, the time nonlocal transport parameters in the F-MIM model are predictable for alluvial settings, improving the predictability of time nonlocal transport models.

Appendix A: Literature Review of Time and Space Nonlocal Transport Models

Anomalous diffusion characterized by the nonlinear scaling of plume variance develops because of nonlocal dependence on either past conditions (time) [*Cushman*, 1991; *Cushman et al*., 1994; *Schumer et al*., 2003a; *Dentz et al*., 2004; *Dentz and Tartakovsky*, 2006] or far upstream (space) concentrations [*Cushman and Ginn*, 2000; *Molz et al*., 2002; *Schumer et al*., 2001; *Zhang et al*., 2007a]. The temporal nonlocality can be physically attributed to mass transfer of solute between relatively immobile and mobile phases [*Haggerty et al*., 2000; *Dentz and Berkowitz*, 2003], while the spatial nonlocality is due to long-range dependence of flow paths [*Benson et al*., 2001; *del-Castillo-Negrete et al*., 2005; *Zhang et al*., 2007b; *Bolster et al*., 2010]. While the space and time nonlocal formulations may simulate similar aspects of plume growth, there are fundamental differences. For example, purely space nonlocal models cannot account for the loss of mobile mass, while the time nonlocal methods usually cannot account for early arrivals. Therefore, a physical model combining temporal and spatial nonlocality might be needed for some cases, as shown by applications in this study.

Three nonlocal techniques have been sufficiently developed to be useful to the general hydrology community. These techniques include the (single- and) multiple-rate mass transfer (MRMT) method [e.g., *Haggerty and Gorelick*, 1995; *Harvey and Gorelick*, 1995, 2000; *Haggerty et al*., 2000], the continuous time random walk (CTRW) framework developed by *Berkowitz* and coworkers [*Berkowitz et al*., 2006; *Edery et al*., 2014], and the fADE method discussed in the main text [*Benson et al*., 2000]. The MRMT and CTRW techniques are time nonlocal models and they generally attribute anomalous transport to the long period of time during which solute "particles" move slowly; however, when they are in a relatively mobile phase, the solutes undergo Fickian transport governed by the traditional ADE. The space fADE, which is a space nonlocal model, adds non-Gaussian transport and therefore directly models early arrivals while the solutes are in a mobile state. In any case, all nonlocal methods replace the (infinitely) fine local scale velocity with a simpler statistical description of the amount of time it takes a particle to move a random distance. Typically this adds several parameters to the governing equation but increases parsimony by replacing detailed velocity information.

The CTRW framework and the fADE method have been useful for fitting laboratory column tests [*Pachepsky et al*., 2000; *Cortis and Berkowitz*, 2004] and 1-D or 2-D projections of field data [*Berkowitz and Scher*, 1998; *Benson et al*., 2000, 2001; *Zhang et al*., 2008]. The well-known MRMT approach, including single-rate subsets, have been successfully used for decades [*Coats and Smith*, 1964; *Carrera et al*., 1998; *Feehley et al*., 2000; *Swanson et al*., 2015, among many others].

Recently, *Cvetkovic* [2011] found that a waiting time density following the tempered one-sided stable might be a universal model for hydrological transport. *Hansen and Berkowitz* [2014] found that the Pareto transition time distributions can fit two sets of existing experimental data. *Zhang et al*. [2006] demonstrated that the summation of Pareto random variables converges to the stable density, leading to the fADE model. If the waiting time for solute particles between two jumps is a random variable, then the scaling limit of the random process is either the time fADE (if the mean of the random waiting times, *M*, diverges) or the tempered stable fADE (if *M* converges) [*Meerschaert and Scheffler*, 2008]. In other words, these studies implied the applicability of a temporally tempered fADE model to capture anomalous diffusion due to nonlocal transport in time, which is consistent with the finding by *Meerschaert et al*. [2008]. This popular time nonlocal model is compared with the model used in this study in section 4.

Appendix B: Subordination to Regional Flow

The mathematical method "Subordination" [*Feller*, 1971] was used by *Baeumer et al*. [2001] to randomize the time variable in standard transport models to represent the operational time experienced by each individual tracer particle. For the advection-driven transport process, the standard governing equation is

$$\frac{\partial C(\vec{x},t)}{\partial t} = -\nabla[\vec{v}\, C(\vec{x},t)]\,, \tag{B1}$$

with the initial condition $C(\vec{x},t=0)=C_0(\vec{x})$. One can define a subordinator g_ψ, whose Fourier transform satisfies [see *Baeumer et al*., 2014, equation (3)]:

$$\frac{\partial \hat{g}_\psi}{\partial t} = \psi(ik)\,\hat{g}_\psi\,, \tag{B2}$$

with the initial condition $\hat{g}_\psi = 1$, and $\psi(ik) = -ik$ is the log-characteristic function of the subordinating process.

The subordinated flow corresponding to equation (B1) is governed by [see *Baeumer et al.*, 2014, equation (4)]:

$$\frac{\partial C}{\partial t} = \psi(\nabla_{\vec{v}})C\,, \tag{B3}$$

where $\psi(\nabla_{\vec{v}})$ is a differential operator defined through a functional calculus [*Baeumer et al.*, 2009]. Equation (B3) can be expanded as (for a simplified version, see *Baeumer et al.*, [2014, equation (11)])

$$\frac{\partial C}{\partial t} = -\nabla(\vec{v}C) + \sigma(\nabla_{\vec{v}})^{\alpha} C\,. \tag{B4}$$

Baeumer et al. [2014] showed that, by definition, if $C(\vec{x}, t)$ is the solution of equation (B1), then

$$C_\psi(\vec{x}, t) = \int g_\psi(t, \tau)\, C(\vec{x}, \tau)\, d\tau, \tag{B5}$$

is the solution of equation (B3). In other words, the solution of equation (B4) can be obtained by subordination transforming the solution to equation (B1).

Appendix C: Property of the Time fADE (28)

First, we emphasize again here that the time fADE model (28) is also a MRMT model. The standard MRMT model with the first-order mass transfer can be written as [see also *Schumer et al.*, 2003a, equation (6)]:

$$\frac{\partial C_m}{\partial t} + \beta \frac{\partial C_m}{\partial t} * f(t) = -V\frac{\partial C_m}{\partial x} + D\frac{\partial^2 C_m}{\partial x^2} - \beta f(t)\, m_0\, \delta(x)\,, \tag{C1a}$$

$$C_{im}(\vec{x}, t) = \int_0^t f(t-s)\, C_m(\vec{x}, s)\, ds\,, \tag{C1b}$$

where $\delta()$ is the Dirac delta function and m_0 denotes the initial mass (which is assumed to be located in the mobile phase). Taking Fourier-Laplace transforms in equation (C1a) yields:

$$\hat{\tilde{C}}_m(k, s) = \frac{m_0}{s + \beta s \tilde{f}(s) + Vik + Dk^2}\,, \tag{C2}$$

which can be rearranged to

$$s\hat{\tilde{C}}_m(k, s) - m_0 + \beta s \tilde{f}(s)\hat{\tilde{C}}_m(k, s) = [-Vik + D(ik)^2]\hat{\tilde{C}}_m(k, s)\,. \tag{C3}$$

Assuming exponentially tempered power-law waiting times, *Meerschaert et al.* [2008] proposed the following memory function (in the Laplace domain):

$$\tilde{f}(s) = s^{-1}(\lambda_T + s)^{\gamma} - s^{-1}\lambda_T^{\gamma}\,. \tag{C4}$$

Inserting the memory function (C4) into equation (C3) and then taking the inverse Fourier-Laplace transforms, one obtains the mobile equation:

$$\frac{\partial C_m}{\partial t} + \beta e^{-\lambda_T t}\frac{\partial^{\gamma}\left[e^{\lambda_T t} C_m\right]}{\partial t^{\gamma}} = -V\frac{\partial C_m}{\partial x} + D\frac{\partial^2 C_m}{\partial x^2}\,, \tag{C5}$$

which is equation (28a). Similarly, we can obtain the governing equation for immobile solutes (following the same procedure shown in *Meerschaert et al.* [2008]), which is the same as equation (28b). Therefore, the time fADE model (28) is actually the MRMT model (C1) where the memory function is a tempered stable density.

Second, we emphasize here again that model (28) assumes the tempered stable density for solute waiting times. *Cvetkovic* [2011] also found that the water residence time in hydrological transport typically distributes as the tempered one-sided stable (TOSS) density, which was first proposed by *Cvetkovic and Haggerty* [2002] for solute transport with exchange in disordered media (see *Cvetkovic and Haggerty* [2002], equation (10), which defines the "truncated stable density"). The TOSS density enables efficient computations of

tracer transport subject to kinetically controlled mass transfer. *Cvetkovic* [2011] found that the TOSS distribution, expressed by equation (3) in *Cvetkovic* [2011], recovers virtually all residence time distributions considered in the literature for hydrological transport. This TOSS density, which is the asymmetric (one-sided), exponentially truncated stable density, is identical to the tempered stable density assumed by the memory function (C4). Since the time fADE or MRMT model (28) is equivalent to the model of *Cvetkovic* [2011], applications of (28) in section 4 provide a framework for further verifying the TOSS density model using real-world transport data.

Appendix D: Mechanism and Detection of Early Arrivals in Geological Media

Mechanism for early arrivals may include: (1) a heavy tailed and long-range dependent hydraulic conductivity for porous media [*Benson et al*., 2001; *Herrick et al*., 2002; *Kohlbecker et al*., 2006; *Dentz and Bolster*, 2010], or (2) power-law distributed, uncorrelated velocities [*Dentz and Bolster*, 2010]. *Zhang et al*. [2014b] also found that the spatial correlation of high-permeable deposits is critical, in order to facilitate fast jumps through a heterogeneous porous medium. This mechanism differs from that for retention, where the overall retention is simply the summation of contribution from each immobile phase and therefore the late-time BTC is not very sensitive to the exact location of immobile blocks on the pathway of solute particles [*Zhang et al*., 2009]. This mechanism also explains the weak leading edge of particle plumes observed in Case 2 (i.e., the hydrofacies model discussed in section 4.2), because the transition probability defining the spatial correlation of hydrofacies is not heavy-tailed but a summation of several exponential functions. The above mechanism also explains why retention is much more commonly observed than early arrivals in column transport experiments. When natural soils are repacked in a column, the intrinsic heterogeneity and internal connectivity (such as interconnected macropores) tend to be disturbed, removing the original fast jumps along preferential flow pathes. Meanwhile, the soil matrix zones still cause retention, although the structure can be reorganized. This explains why Case 5 (leaching experiments along soil columns in section 4.5) discussed above does not show any sign of early arrivals.

For regional-scale fractured media (such as Cases 3 and 4), the fracture properties (including the transmissivity, length, and density) affect early arrivals [*Reeves et al*., 2008a, 2008b]. For a local-scale single fracture (Case 4), the combination of non-Darcian flow and boundary layer dispersion may induce early arrivals [*Qian et al*., 2011].

The above analysis shows that retention and early arrivals are driven by different mechanisms, and therefore can be modeled separately in a physical model, such as our two-step Lagrangian scheme. In addition, fast jumps in heterogenous media are originated from upstream dispersive fluxes, a space nonlocal process fitting well the physical interpretation of the space fractional derivative.

In addition, the detection of early arrivals is constrained by the travel distance and the detection limit of tracers. First, at a spatial scale much larger than $1/\lambda_L$ (where λ_L is the space truncation parameter), the upper-truncated fast jumps converges to Fickian diffusion. This can be seen from Case 2 (i.e., the hydrofacies model), where $1/\lambda_L$ is small and therefore the leading edge of plumes can be approximated by the time nonlocal transport model after particles travel a long distance. Second, the mass of early arrived tracers can be below the detection limit (see Case 3 discussed above) and therefore may be hard to measure in the field. The F-MIM model (7) helps to identify early arrivals in real-world problems, since the space fractional derivative term in (7) can efficiently model the transition from non-Fickian to Fickian diffusion, and provide numerical solutions for early arrivals that might be missed in measurements.

Acknowledgments
This work was supported by the National Science Foundation under DMS-1025417, EAR-1344280, and DMS-1460319, and partially by the University of Alabama Research Grant Committee. The data for this paper are available upon request from the corresponding author, Yong Zhang, at yzhang264@ua.edu. This paper does not necessary reflect the view of the funding agencies. We thank the editors and three reviewers for suggestions that improved the presentation of this work.

References

Baeumer, B., D. A. Benson, M. M. Meerschaert, and S. W. Wheatcraft (2001), Subordinated advection-dispersion equation for contaminant transport, *Water Resour. Res.*, *37*(6), 1543–1550.

Baeumer, B., M. Haase, and M. Kovacs (2009), Unbounded functional calculus for bounded group with applications, *J. Evol. Equations*, *9*, 171–195.

Baeumer, B., Y. Zhang, and R. Schumer (2014), Incorporating super-diffusion due to sub-grid heterogeneity to capture non-Fickian transport, *Ground Water*, doi:10.1111/gwat.12267.

Benson, D. A., and M. M. Meerschaert (2008), Simulation of chemical reaction via particle tracking: Diffusion-limited versus thermodynamic rate-limited regimes, *Water Resour. Res.*, *44*, W12202, doi:10.1029/2008WR007111.

Benson, D. A., and M. M. Meerschaert (2009), A simple and efficient random walk solution of multi-rate mobile/immobile mass transport equations, *Adv. Water Resour.*, *32*, 532–539.

Benson, D. A., S. W. Wheatcraft, and M. M. Meerschaert (2000), Application of a fractional advectiondispersion equation, *Water Resour. Res.*, *36*(6), 1403–1412.

Benson, D. A., R. Schumer, M. M. Meerschaert, and S. W. Wheatcraft (2001), Fractional dispersion, Lévy motion, and the MADE tracer tests, *Transp. Porous Media*, *42*(1/2), 211–240.
Benson, D. A., C. Tadjeran, M. M. Meerschaert, I. Farnham, and G. Pohll (2004), Radial fractional-order dispersion through fractured rock, *Water Resour. Res.*, *40*, W12416, doi:10.1029/2004WR003314.
Berkowitz, B. (2002), Characterizing flow and transport in fractured geological media: A review, *Adv. Water Resour.*, *25*, 861–884.
Berkowitz, B., and H. Scher (1998), Theory of anomalous chemical transport in random fracture networks, *Phys. Rev. E*, *57*(5), 5858–5869.
Berkowitz, B., A. Cortis, M. Dentz, and H. Scher (2006), Modeling non-Fickian transport on geological formations as a continuous time random walk, *Rev. Geophys.*, *44*, RG2003, doi:10.1029/2005RG000178.
Bolster, D., D. A. Benson, T. Le Borgne, and M. Dentz (2010), Anomalous mixing and reaction induced by superdiffusive nonlocal transport, *Phys. Rev. E*, *82*(2), 021119.
Bromly, M., and C. Hinz (2004), Non-Fickian transport in homogeneous unsaturated repacked sand, *Water Resour. Res.*, *40*, W07402, doi:10.1029/2003WR002579.
Carrera, J., X. Sanchez-Vila, I. I. Benet, A. Medina, G. Galarza, and J. Guimera (1998), On matrix diffusion: Formulations, solution methods, and qualitative effects, *Hydrogeol. J.*, *6*, 178–190.
Chen, Z., J. Z. Qian, and H. Qin (2011), Experimental study of the non-Darcy flow and solute transport in a channeled single fracture, *J. Hydrodyn.*, *23*(6), 745–751.
Cinlar, E. (1969), Markov renewal theory, *Adv. Appl. Probab.*, *1*(2), 123–187.
Coats, K. H., and B. D. Smith (1964), Dead-end pore volume and dispersion in porous media, *Soc. Pet. Eng. J.*, *3*, 73–84.
Cortis, A., and B. Berkowitz (2004), Anomalous transport in "classical" soil and sand columns, *Soil Sci. Soc. Am. J.*, *68*, 1539–1548.
Cushman, J. H. (1991), On diffusion in fractal porous media, *Water Resour. Res.*, *27*(4), 643–644.
Cushman, J. H., and T. R. Ginn (2000), Fractional advection-dispersion equation: A classical mass balance with convolution-Fickian flux, *Water Resour. Res.*, *36*(12), 3763–3766.
Cushman, J. H., B. X. Hu, and T. R. Ginn (1994), Nonequilibrium statistical mechanics of preasymptotic dispersion, *J. Stat. Phys.*, *75*(5/6), 859–878.
Cvetkovic, V. (2011), The tempered one-sided stable density: A universal model for hydrological transport?, *Environ. Res. Lett.*, *6*, 034008, doi:10.1088/1748–9326/6/3/034008.
Cvetkovic, V., and R. Haggerty (2002), Transport with exchange in disordered media, *Phys. Rev. E*, *65*, 051308.
Czernuszenko, W., P. M. Rowinski, and A. Sukhodolov (1998), Experimental and numerical validation of the dead-zone model for longitudinal dispersion in rivers, *J. Hydraul. Res.*, *36*(2), 269–280.
Dean, C. A., and P. W. Reimus (2008), Effective Kd values for radionuclides in Yucca Mountain saturated alluvium, in *Proceedings of the 12th International High Level Radioactive Waste Management Conference (IHLRWM)*, pp. 171–178, Am. Nucl. Soc., LaGrange Park, Ill.
Delay, F., P. Ackerer, and C. Danquigny (2005), Simulating solute transport in porous or fractured formations using random walk particle tracking, *Vadose Zone J.*, *4*(2), 360–379.
del-Castillo-Negrete, D., B. A. Carreras, and V. E. Lynch (2005), Nondiffusive transport in plasma turbulence: A fractional diffusion approach, *Phys. Rev. Lett.*, *94*(6), 065003.
Deng, Z.-Q., V. P. Singh, and L. Bengtsson (2004), Numerical solution of fractional advection-dispersion equation, *J. Hydraul. Eng.*, *130*(5), 422–431.
Deng, Z.-Q., L. Bengtsson, and V. P. Singh (2006), Parameter estimation for fractional dispersion model for rivers, *Environ. Fluid Mech.*, *6*, 451–475.
Dentz, M., and B. Berkowitz (2003), Transport behavior of a passive solute in continuous time random walks and multirate mass transfer, *Water Resour. Res.*, *39*(5), 1111, doi:10.1029/2001WR001163.
Dentz, M., and D. Bolster (2010), Distribution- versus correlation-induced anomalous transport in quenched random velocity fields, *Phys. Rev. Lett.*, *105*, 244301.
Dentz, M., and D. M. Tartakovsky (2006), Delay mechanisms of non-Fickian transport in heterogeneous media, *Geophys. Res. Lett.*, *33*, L16406, doi:10.1029/2006GL027054.
Dentz, M., A. Cortis, H. Scher, and B. Berkowitz (2004), Time behavior of solute transport in heterogeneous media: Transition from anomalous to normal transport, *Adv. Water Resour.*, *27*, 155–173.
Drummond, J. D., A. F. Aubeneau, and A. I. Packman (2014), Stochastic modeling of fine particulate organic carbon dynamics in rivers, *Water Resour. Res.*, *50*, 4341–4356, doi:10.1002/2013WR014665.
Edery, Y., H. Scher, and B. Berkowitz (2009), Modeling bimolecular reactions and transport in porous media, *Geophys. Res. Lett.*, *36*, L02407, doi:10.1029/2008GL036381.
Edery, Y., H. Scher, and B. Berkowitz (2010), Particle tracking model of bimolecular reactive transport in porous media, *Water Resour. Res.*, *46*, W07524, doi:10.1029/2009WR009017.
Edery, Y., A. Guadagnini, H. Scher, and B. Berkowitz (2014), Origins of anomalous transport in disordered media: Structural and dynamic controls, *Water Resour. Res.*, *50*, 1490–1505, doi:10.1002/2013WR015111.
Feehley, C. E., C. M. Zheng, and F. J. Molz (2000), A dual-domain mass transfer approach for modeling solute transport in heterogeneous aquifers: Application to the Macrodispersion Experiment (MADE) site, *Water Resour. Res.*, *36*(9), 2501–2515.
Feller, W. (1971), *An Introduction to Probability Theory and Its Applications*, vol. II, 2nd ed., John Wiley, N. Y.
Fisher, A. J., D. A. Green, and A. V. Metcalfe (2010), Managing river flow in arid regions with matrix analytic methods, *J. Hydrol.*, *382*(1), 128–137.
Fogg, G. E., S. F. Carle, and C. T. Green (2000), A connected-network paradigm for the alluvial aquifer system, in *Theory, Modeling and Field Investigation in Hydrogeology: A Special Volume in Honor of Schlomo P. Neumans 60th Birthday, Geol. Soc. Am. Spec. Publ.*, edited by D. Zhang, Geol. Soc. Am. Spec. Pap., 348, pp. 25–42, Boulder, Colo.
Fuller, C. C., J. A. Davis, and G. A. Waychunas (1993), Surface chemistry of ferrihydrite: Part 2: Kinetics of arsenate adsorption and coprecipitation, *Geochim. Cosmochim. Acta*, *57*, 2271–2282.
Golder, J., M. Joelson, M. C. Neel, and L. Dl Pietro (2014), A time fractional model to represent rainfall process, *Water Sci. Eng.*, *7*(1), 32–40.
González-Pinzón, R., R. Haggerty, and M. Dentz (2013), Scaling and predicting solute transport processes in streams, *Water Resour. Res.*, *49*, 4071–4088, doi:10.1002/wrcr.20280.
Green, T. C., Y. Zhang, B. C. Jurgens, J. F. Starn, and M. K. Landon (2014), Accuracy of travel time distribution (TTD) models as affected by TTD complexity, observation errors, and model and tracer selection, *Water Resour. Res.*, *50*, 6191–6213, doi:10.1002/2014WR015625.
Haggerty, R., and S. M. Gorelick (1995), Multiple-rate mass transfer for modeling diffusion and surface reactions in media with pore-scale heterogeneity, *Water Resour. Res.*, *31*(10), 2383–2400.

Haggerty, R., S. A. McKenna, and L. C. Meigs (2000), On the late-time behavior of tracer test breakthrough curves, *Water Resour. Res.*, *36*(12), 3467–3479.
Hansen, S. K., and B. Berkowitz (2014), Interpretation and nonuniqueness of CTRW transition distributions: Insights from an alternative solute transport formulation, *Adv. Water Resour.*, *74*, 54–63.
Harbaugh, A. W. (2005), *MODFLOW-2005*, The U.S. Geological Survey modular ground-water model—The Ground-water flow process, *U.S. Geol. Surv. Tech. Methods*, 6-A16, 253 pp.
Harvey, C. F., and S. M. Gorelick (1995), Temporal moment generating equations: Modeling transport and mass transfer in heterogeneous aquifers, *Water Resour. Res.*, *31*(8), 1895–1911.
Harvey, C. F., and S. M. Gorelick (2000), Rate-limited mass transfer or macrodispersion: Which dominates plume evolution at the Macrodispersion Experiment (MADE) site?, *Water Resour. Res.*, *36*(3), 637–650.
Heidari, P., and L. Li (2014), Solute transport in low-heterogeneity sand boxes: The role of correlation length and permeability variance, *Water Resour. Res.*, *50*, 8240–8264, doi:10.1002/2013WR014654.
Herrick, M.G., D. A. Benson, M. M. Meerschaert, and K. R. McCall (2002), Hydraulic conductivity, velocity, and the order of the fractional dispersion derivative in a highly heterogeneous system, *Water Resour. Res.*, *38*(11), 1227, doi:10.1029/2001WR000914.
Herrmann, R. (2011), *Fractional Calculus: An Introduction for Physicists*, 276 pp., World Sci., Singapore.
Houssais, M., and E. Lajeunesse (2012), Bedload transport of a bimodal sediment bed, *J. Geophys. Res.*, *117*, F04015, doi:10.1029/2012JF002490.
Hunt, A. G., R. P. Ewing, and R. Horton (2013), What's wrong with soil physics?, *Soil Sci. Soc. Am.*, *77*(6), 1877–1887.
Jennings, G. I., D. Prigge, S. Carney, S. Karni, J. B. Rauch, and R. Abgrall (2014), Water wave propagation in unbounded domains. Part II: Numerical methods for fractional PDEs, *J. Comput. Phys.*, *275*, 443–458.
Kendall, D. R., and J. A. Dracup (1992), On the generation of drought events using an alternating renewal-reward model, *Stochastic Hydrol. Hydraul.*, *6*(1), 55–68.
Kilbas, A. A., H. H. Srivastava, and J. J. Trujillo (2006), *Theory and Applications of Fractional Differential Equations*, 540 pp., Elsevier, Amsterdam, Netherlands.
Kim, S., and M. L. Kavvas (2006), Generalized Fick's law and fractional ADE for pollutant transport in a river: Detailed derivation, *J. Hydrol. Eng.*, *11*(1), 80–83.
Kohlbecker, M., S. W. Wheatcraft, and M. M. Meerschaert (2006), Heavy tailed log hydraulic conductivity distributions imply heavy tailed log velocity distributions, *Water Resour. Res.*, *42*, W04411, doi:10.1029/2004WR003815.
Kosakowski, G. (2004), Anomalous transport of colloids and solutes in a shear zone, *J. Contam. Hydrol.*, *72*(104), 23–46.
LaBolle, E. M., and G. E. Fogg (2001), Role of molecular diffusion in contaminant migration and recovery in an alluvial aquifer system, *Transp. Porous Media*, *42*, 155–179.
LaBolle, E. M., G. E. Fogg, and A. F. B. Tompson (1996), Random-walk simulation of transport in heterogeneous porous media: Local mass-conservation problem and implementation methods, *Water Resour. Res.*, *32*(3), 583–393.
LaBolle, E. M., J. Quastel, and G. E. Fogg (1998), Diffusion theory for transport in porous media: Transition-probability densities of diffusion processes corresponding to advection-dispersion equations, *Water Resour. Res.*, *34*(7), 1685–1693.
Le Borgne, T., and P. Gouze (2008), Non-Fickian dispersion in porous media: 2. Model validation from measurements at different scales, *Water Resour. Res.*, *44*, W06427, doi:10.1029/2007WR006279.
Le Borgne, T., M. Dentz, and J. Carrera (2008), Lagrangian statistical model for transport in highly heterogeneous velocity fields, *Phys. Rev. Lett.*, *101*, 090601.
Levy, M., and B. Berkowitz (2003), Measurement and analysis of non-Fickian dispersion in heterogeneous porous media, *J. Contam. Hydrol.*, *64*, 203–226.
Meerschaert, M. M., and H. P. Scheffler (2008), Triangular array limits for continuous time random walks, *Stochastic Processes Appl.*, *118*(9), 1606–1633.
Meerschaert, M. M., D. A. Benson, and B. Baeumer (2001), Operator Lévy motion and multiscaling anomalous diffusion, *Phys. Rev. E*, *63*, 021112, doi:10.1103/PhysRevE.63.021112.
Meerschaert, M. M., Y. Zhang, and B. Baeumer (2008), Tempered anomalous diffusion in heterogeneous systems, *Geophys. Res. Lett.*, *35*, L17403, doi:10.1029/2008GL034899.
Meerschaert, M. M., Y. Zhang, and B. Baeumer (2010), Particle tracking for fractional diffusion with two time scales, *Comput. Math. Appl.*, *59*, 1078–1086.
Metzler, R., and J. Klafter (2000), The random walk's guide to anomalous diffusion: A fractional dynamics approach, *Phys. Rep.*, *339*(1), 1–77.
Metzler, R., and J. Klafter (2004), The restaurant at the end of the random walk: Recent development in fractional dynamics of anomalous transport processes, *J. Phys.*, *37*, R161–R208.
Michalak, A. M., and P. K. Kitanidis (2000), Macroscopic behaviour and random-walk particle tracking of kinetically sorbing solutes, *Water Resour. Res.*, *36*(8), 2133–2146.
Molz F. J., G. J. Fix, and S. L. Lu (2002), A physical interpretation for the fractional derivative in Lévy diffusion, *Appl. Math. Lett.*, *15*, 907–911.
O'Reilly, S. E., D. G. Strawn, and D. L. Sparks (2001), Residence time effects on arsenate adsorption/desorption mechanisms on goethite, *Soil Sci. Soc. Am. J.*, *65*, 67–77.
Pachepsky, Y., D. Timlin, and D. A. Benson (2000), Transport of water and solutes in soils as in fractal porous media, *Soil Sci. Soc. Am. J.*, *56*, 51–75.
Pedretti, D., D. Fernàndez-Garcia, D. Bolster D, and X. Sanchez-Vila (2013), On the formation of breakthrough curves tailing during convergent flow tracer tests in three-dimensional heterogeneous aquifers, *Water Resour. Res.*, *49*, 4157–4173, doi:10.1002/wrcr.20330.
Qi, Y. Q., and R. J. Donahoe (2011), Modeling arsenic sorption in the subsurface with a dual-site model, *Ground Water*, *49*(2), 219–226.
Qian, J. Z., H. B. Zhan, Z. Chen, and H. Ye (2011), Experimental study of solute transport under non-Darcian flow in a single fracture, *J. Hydrol.*, *399*, 246–254.
Reeves, D. M., D. A. Benson, and M. M. Meerschaert (2008a), Transport of conservative solutes in simulated fracture networks: 1. Synthetic fracture generation, *Water Resour. Res.*, *44*, W05404, doi:10.1029/2007WR006069.
Reeves, D. M., D. A. Benson, M. M. Meerschaert, and H. P. Scheffler (2008b), Transport of conservative solutes in simulated fracture networks: 2. Ensemble solute transport and the correspondence to operator stable limit distributions, *Water Resour. Res.*, *44*, W05410, doi:10.1029/2008WR006858.
Reimus, P., G. Pohll, T. Mihevc, J. Chapman, M. Haga, B. Lyles, S. Kosinski, R. Niswonger, and P. Sanders (2003), Testing and parameterizing a conceptual model for solute transport in a fractured granite using multiple tracers in a forced-gradient test, *Water Resour. Res.*, *39*(12), 1356, doi:10.1029/2002WR001597.

Ronayne, M. J. (2013), Influence of conduit network geometry on solute transport in karst aquifers with a permeable matrix, *Adv. Water Resour.*, *56*, 27–34.
Ross, S. M. (1983), *Stochastic Processes*, John Wiley, N. Y.
Salamon, P., D. Fernàndez-Garcia, and J. J. Gómez-Hernández (2006), Modeling mass transfer processes using random walk particle tracking, *Water Resour. Res.*, *42*, W11417, doi:10.1029/2006WR004927.
Schumer, R., D. A. Benson, M. M. Meerschaert and B. Baeumer (2001), Eulerian derivation of the fractional advection-dispersion equation, *J. Contam. Hydrol.*, *48*, 69–88.
Schumer, R., D. A. Benson, M. M. Meerschaert, and B. Baeumer (2003a), Fractal mobile/immobile solute transport, *Water Resour. Res.*, *39*(10), 1296, doi:10.1029/2003WR002141.
Schumer, R., D. A. Benson, M. M. Meerschaert, and B. Baeumer (2003b), Multiscaling fractional advection-dispersion equations and their solutions, *Water Resour. Res.*, *39*(1), 1022, doi:10.1029/2001WR001229.
Schumer, R., M. M. Meerschaert, and B. Baeumer (2009), Fractional advection-dispersion equation for modeling transport at the Earth surface, *J. Geophy. Res.*, *114*, F00A07, doi:10.1029/2008JF001246.
Sokolov, I. M., and R. Metzler (2004), Non-uniqueness of the first passage time density of Levy random processes, *J. Phys. A Math. Gen.*, *37*(46), L609–L615, doi:10.1088/0305–4470/37/46/l02.
Stark, C., E. Foufoula-Georgiou, and V. Ganti (2009), A nonlocal theory of sediment buffering and bedrock channel evolution, *J. Geophys. Res.*, *114*, F01029, doi:10.1029/2008JF000981.
Sun, H., D. Chen, Y. Zhang, Y., and L. Chen (2015), Understanding partial bed-load transport: Experiments and stochastic model analysis, *J. Hydrol.*, *521*, 196–204.
Swanson, R. D., A. Binley, K. Keating, S. France, G. Osterman, F. D. Day-Lewis, and K. Singha (2015), Anomalous solute transport in saturated porous media: Relating transport model parameters to electrical and nuclear magnetic resonance properties, *Water Res. Res.*, *51*, 1264–1283, doi:10.1002/2014WR015284.
Tarasov, V. E. (2014), Flow of fractal fluid in pipes: Non-integer dimensional space approach, *Chaos Solitons Fractals*, *67*, 26–37.
Tijms, H. C. (2003), *A First Course in Stochastic Models*, John Wiley, Chichester, U. K.
Tsang, C. F., and I. Neretnieks (1998), Flow channeling in heterogeneous fractured rocks, *Rev. Geophys.*, *36*(2), 275–298.
Uffink, G., A. Elfeki, M. Dekking, J. Bruining, and C. Kraaikamp (2012), Understanding the non-Gaussian nature of linear reactive solute transport in 1D and 2D, *Transp. Porous Media*, *91*, 547–571.
Zhang, Y., D. A. Benson, M. M. Meerschaert, E. M. LaBolle, and H. P. Scheffler (2006), Random walk approximation of fractional-order multiscaling anomalous diffusion, *Phys. Rev. E*, *74*, 026706, doi:10.1103/PhysRevE.74.026706.
Zhang, Y., D. A. Benson, M. M. Meerschaert, and E. M. LaBolle (2007a), Space-fractional advection-dispersion equations with variable parameters: Diverse formulas, numerical solutions, and application to the MADE-site data, *Water Resour. Res.*, *43*, W05439, doi:10.1029/2006WR004912.
Zhang, Y., D. A. Benson, and B. Baeumer (2007b), Predicting the tails of breakthrough curves in regional-scale alluvial systems, *Ground Water*, *45*(4), 473–484.
Zhang, Y., M. M. Meerschaert, and B. Baeumer (2008), Particle tracking for time-fractional diffusion, *Phys. Rev. E*, *78*, 036705, doi:10.1103/PhysRevE.78.036705.
Zhang, Y., D. A. Benson, and D. M. Reeves (2009), Time and space nonlocalities underlying fractional-derivative models: Distinction and literature review of field applications, *Adv. Water Resour.*, *32*(4), 561–581.
Zhang, Y., D. M. Reeves, K. Pohlmann, J. B. Chapman, and C. E. Russell (2013), Fractional dynamics of tracer transport in fractured media from local to regional scales, *Cent. Eur. J. Phys.*, *11*(6), 634–645, doi:10.2478/s11534-013-0200-x.
Zhang, Y., J. Z. Qian, C. Papelis, P. T. Sun, and Z. B. Yu (2014a), Improved understanding of bimolecular reactions in deceptively simple homogeneous media: From laboratory experiments to Lagrangian quantification, *Water Resour. Res.*, *50*, 1704–1715, doi:10.1002/2013WR014711.
Zhang, Y., C. T. Green, and B. Baeumer (2014b), Linking aquifer spatial properties and non-Fickian transport in mobile-immobile like alluvial settings, *J. Hydrol.*, *512*, 315–331.